Deterministic and stochastic control of kirigami topology

Siheng Chen[a,1], Gary P. T. Choi[a,1], and L. Mahadevan[a,b,c,d,2]

[a]John A. Paulson School of Engineering and Applied Sciences, Harvard University, Cambridge, MA 02138; [b]Department of Physics, Harvard University, Cambridge, MA 02138; [c]Department of Organismic and Evolutionary Biology, Harvard University, Cambridge, MA 02138; and [d]Kavli Institute for Bionano Science and Technology, Harvard University, Cambridge, MA 02138

Edited by John A. Rogers, Northwestern University, Evanston, IL, and approved January 10, 2020 (received for review October 5, 2019)

Kirigami, the creative art of paper cutting, is a promising paradigm for mechanical metamaterials. However, to make kirigami-inspired structures a reality requires controlling the topology of kirigami to achieve connectivity and rigidity. We address this question by deriving the maximum number of cuts (minimum number of links) that still allow us to preserve global rigidity and connectivity of the kirigami. A deterministic hierarchical construction method yields an efficient topological way to control both the number of connected pieces and the total degrees of freedom. A statistical approach to the control of rigidity and connectivity in kirigami with random cuts complements the deterministic pathway, and shows that both the number of connected pieces and the degrees of freedom show percolation transitions as a function of the density of cuts (links). Together, this provides a general framework for the control of rigidity and connectivity in planar kirigami.

kirigami | rigidity | connectivity | linkage

Kirigami, the traditional art of paper cutting, has inspired the design of a new class of metamaterials with novel shapes (1–5), electronic/mechanical properties (6–11), and auxetic behavior (12–14). In these studies, typically, the geometry (the shape of the deployed kirigami) and the topology of cuts (spatial distributions of the cuts) are prescribed. Recently, we have shown how to modulate the geometry of the kirigami structures (15) by varying the size and orientation of the cuts to solve the inverse problem of designing kirigami tessellations that can be deployed to approximate given two- and three-dimensional (3D) shapes. However, in these and other studies, the topology of the cuts is not a variable that can be changed to achieve a prescribed shape or mechanical response. Here, we relax this constraint and allow the topology of the kirigami structures to be a design variable that we can control in either a deterministic or a stochastic way to achieve a given connectivity or rigidity in aperiodic planar structures.

We start by considering cutting a thin sheet of material (width = height = l) to obtain a planar kirigami system, that is, an initial structure that has cuts that allow it to be transformed into a new shape using local rotations with no energy cost. Since cuts at random locations with random directions and random lengths are unlikely to lead to a system that can respond via purely rotational modes, we start with a quad kirigami structure (1), a simple fourfold symmetric auxetic structure as shown in Fig. 1*A*. To constrain the infinite phase space of cuts to a finite combination, we adopt the following assumptions: 1) We only allow horizontal and vertical cuts on grid lines with equal spacing d. There are $L = l/d$ horizontal and L vertical grid lines. 2) The sheet is cut along all of the grid lines, except in the vicinity of vertices where the grid lines intersect (Fig. 1*A*). 3) Since kirigami is deployable, the quads need to rotate around their corner hinges, and we assume that the width of hinges is infinitesimally small. Around internal vertices, there are four infinitesimally small segments which we can independently decide to cut or not, as illustrated by the dashed lines marked as ⑤ to ⑧ in Fig. 1*A*. For boundary vertices, there is only one segment (① to ④ in Fig. 1*A*). 4) The quads connected by the corner hinges can rotate freely without any energy. These assumptions and simplifications allow us to transform the cutting problem into a linkage problem, as shown in Fig. 1*B*, where all of the quads are separated, and each pair of neighboring corners (nodes) of quads can be connected via a link. This is a one-to-one mapping, as each link in Fig. 1*B* has a unique corresponding segment for cutting in Fig. 1*A*. Note that the links do not have actual length—they only force the corners of two quads to be connected (with the same spatial coordinates). With this setup, the problem of cutting to derive a kirigami structure is converted to choosing certain number of links among the $4(L-1)^2 + 4(L-1) = 4L(L-1)$ links to be connected. By adding and removing a specific set of links, one can manipulate the number of degrees of freedom (DoF) and number of connected components (NCC) in the system. Moreover, one can even control the types of floppy modes associated with internal rotational mechanisms (Fig. 1 *C* and *D*) and rigid-body modes coming from additional pieces (connected components) (Fig. 1 *E* and *F*). We note that, while we focus on the quad kirigami, as it is the simplest periodic planar structure, all of our results also hold for kagome kirigami, a sixfold auxetic structure formed by equilateral triangles (*SI Appendix*, section S5).

Having shown the equivalence between connectivity and rigidity of kirigami to that in a linkage, we ask how we might vary the number and spatial distribution of the links to control the number of connected pieces (connectivity) and floppy modes (rigidity) in a kirigamized sheet. We show that prescribing the microscopic cuts in a kirigami tessellation using a hierarchical linkage pattern yields any targeted rigidity and connectivity. Furthermore, in the absence of microscopic control, if we are still able to control just the coarse-grained density of cuts, we show the existence of percolation transitions that allow for the control

Significance

Cutting or gluing of sheets of matter are topological operations that change the size, shape, and mechanical response of the system, as exemplified in kirigami, the art of paper cutting. A constructive approach of adding and removing links either deterministically or stochastically allows us to control the connectivity and rigidity of kirigami. These approaches to controlling kirigami provide guidelines for the design of this class of mechanical metamaterials.

Author contributions: S.C., G.P.T.C., and L.M. conceived the mathematical models and interpreted the computational results; S.C. and G.P.T.C. worked on the theory and simulations in consultation with L.M.; and S.C., G.P.T.C., and L.M. wrote the paper.

The authors declare no competing interest.

This article is a PNAS Direct Submission.

Data deposition: Codes related to this paper have been deposited in the GitHub repository (https://github.com/garyptchoi/kirigami-control).

[1]S.C. and G.P.T.C. contributed equally to this work.

[2]To whom correspondence may be addressed. Email: lmahadev@g.harvard.edu.

This article contains supporting information online at https://www.pnas.org/lookup/suppl/doi:10.1073/pnas.1909164117/-/DCSupplemental.

First published February 13, 2020.

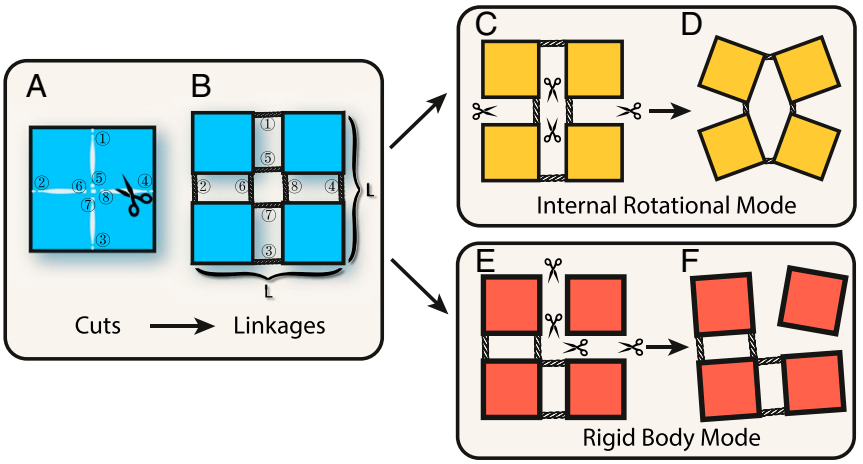

Fig. 1. Quad kirigami and two types of floppy modes. (*A*) The cuts are along edges of quads except at the vertices, so that the pattern is equivalent to a linkage shown in *B*. (*C–F*) Removing certain links can (*C* and *D*) increase the DoF of the structure, adding some internal rotational mechanisms, or (*E* and *F*) increase the NCC, adding translational and rotational rigid-body modes.

of both connectivity and mechanical properties in an exquisitely sensitive way, similar, in some aspects, to rigidity percolation in both planar networks and origami (16–20). (Here we note that the "rigidity" represents the DoF [or number of floppy modes] introduced above, which is different from the "rigidity percolation" transition that describes a global change in the network; e.g., see Fig. 3.)

The connectivity and rigidity of a kirigami tessellation is controlled by the geometrical constraints associated with preserving the four edge lengths and one diagonal length on the four vertices of each quad in a unit cell shown in Fig. 1. These can be written in the form

$$g_{\text{edge}}(\boldsymbol{x_i}, \boldsymbol{x_j}) = \|\boldsymbol{x_i} - \boldsymbol{x_j}\|^2 - d^2 = 0, \quad [1]$$

where node i and node j are connected by an edge in a quad, $i, j \in \{1, \ldots, 4L^2\}$. Additionally, the introduction of rigid links at coincident vertices (Fig. 1) implies that there are constraints on the coordinates of the two vertices for each link connecting node i and node j written as

$$g_{\text{link}_x}(\boldsymbol{x_i}, \boldsymbol{x_j}) = x_{i_1} - x_{j_1} = 0, \quad [2]$$
$$g_{\text{link}_y}(\boldsymbol{x_i}, \boldsymbol{x_j}) = x_{i_2} - x_{j_2} = 0, \quad [3]$$

where $\boldsymbol{x_i} = (x_{i_1}, x_{i_2})$ and $\boldsymbol{x_j} = (x_{j_1}, x_{j_2})$. These sets of constraints determine the range of motions associated with infinitesimal rigidity in terms of the rigidity matrix $\boldsymbol{A}$ where $A_{ij} = \partial g_i / \partial x_j$, so that the DoF is related to the rank of $\boldsymbol{A}$ via the relation (21, 22) (*SI Appendix*, section S1)

$$\text{DoF} = 8L^2 - \text{rank}(A). \quad [4]$$

Kirigami with Prescribed Cuts

Minimum Rigidifying Link Patterns. To address the question of rigidity control with prescribed cuts, we note that the decrease in the total DoF by adding one link is either zero, one, or two (*SI Appendix*, section S1). From a mathematical perspective, each link adds two rows to the rigidity matrix A, and the rank of A can increase by one or two or remain unchanged. Therefore, we can calculate the minimum number of links (denoted as $\delta(L)$) required for rigidifying an $L \times L$ kirigami—having no extra DoF besides the rigid-body motions. Define a minimum rigidifying link pattern (MRP) to be a link pattern (a set of positions for links) that rigidifies the kirigami with exactly $\delta(L)$ links. Note that there are $3L^2$ DoF if all of the links are disconnected, and there are three DoF if all of the links are connected. Since each link reduces the DoF by, at most, two, $\delta(L)$ links can, at most, reduce $2\delta(L)$ DoF and hence $3L^2 - 2\delta(L) \leq 3$. Therefore, $\delta(L) \geq \lceil 3L^2 - 3/2 \rceil$, where $\lceil \cdot \rceil$ is the ceiling function rounding up the number to the nearest integer. Note that $\delta(L)$ might be greater than the lower bound $\lceil 3L^2 - 3/2 \rceil$, since there might be no way that the $\lceil 3L^2 - 3/2 \rceil$ links added are all nonredundant. It is natural to ask whether this lower bound for $\delta(L)$ is achievable (optimal), and, furthermore, is it always possible to find a rigidifying link pattern with exactly $\lceil 3L^2 - 3/2 \rceil$ links?

We give a constructive proof of the optimality of the above lower bound by developing a hierarchical construction method for constructing MRPs for any system size L, where we combine the patterns for small L to construct the patterns for large L. First, we show that, if the lower bound is achievable for two odd numbers $L = L_1$ and $L = L_2$ (i.e., $\delta(L_1) = \lceil 3L_1^2 - 3/2 \rceil$ and $\delta(L_2) = \lceil 3L_2^2 - 3/2 \rceil$), it is also achievable for $L = L_1 L_2$. The key idea is that, if we treat an $L_1 L_2 \times L_1 L_2$ kirigami as $L_2 \times L_2$ large blocks of $L_1 \times L_1$ quads, we can rigidify each large block of $L_1 \times L_1$ quads by an MRP for $L = L_1$, and then link and rigidify all of the $L_2 \times L_2$ large rigid blocks by an MRP for $L = L_2$. This gives a rigidifying link pattern for the $L_1 L_2 \times L_1 L_2$ kirigami, with the total number of links being

$$L_2^2 \delta(L_1) + \delta(L_2) = L_2^2 \left\lceil \frac{3L_1^2 - 3}{2} \right\rceil + \left\lceil \frac{3L_2^2 - 3}{2} \right\rceil$$
$$= L_2^2 \frac{3L_1^2 - 3}{2} + \frac{3L_2^2 - 3}{2} = \frac{3L_1^2 L_2^2 - 3}{2} = \left\lceil \frac{3(L_1 L_2)^2 - 3}{2} \right\rceil. \quad [5]$$

Therefore $\delta(L_1 L_2) = \lceil 3(L_1 L_2)^2 - 3/2 \rceil$, and hence such a link pattern is an MRP for $L = L_1 L_2$. Similarly, if L_1 is odd and L_2 is even, we can show that this relationship still holds (*SI Appendix*, section S1). In fact, using the hierarchical construction method and MRPs for small L (with the optimality of the lower bound for those small L cases proved using the rigidity matrix computation), we can prove that the lower bound $\delta(L)$ is optimal for all L.

Theorem 1 *For all positive integers* L, $\delta(L) = \lceil 3L^2 - 3/2 \rceil$.

Proof. We outline the proof here and provide the details in *SI Appendix*, *Theorems S1–S3*. Our idea is to use perfectly periodic, prime partitions to decompose an $L \times L$ kirigami into blocks of kirigami with smaller size.

In Fig. 2*A*, we explicitly construct MRPs with exactly $\lceil 3L^2 - 3/2 \rceil$ links for $L = 2, 3, 4, 5, 7$, and an auxiliary MRP for

a 3×5 kirigami (*SI Appendix*, section S1). The rigidity of these patterns is verified using the rigidity matrix computation Eq. **4**. Then, with these small patterns, we can use the hierarchical construction to obtain an MRP for any $L = 2^k \prod p_i^{n_i}$, where $k = 0, 1, 2$ and p_i are odd primes satisfying $\delta(p_i) = \lceil 3p_i^2 - 3/2 \rceil$ (Fig. 2*B* and *SI Appendix*, *Theorem S1*).

We further design methods to construct MRPs for all L that is a power of 2 (Fig. 2*C* and *SI Appendix*, *Theorem S2*) and for all odd primes $p \geq 11$ (Fig. 2*D* and *SI Appendix*, *Theorem S3*) by integer partition and hierarchical construction. Ultimately, we can remove all conditions on L and conclude that the $\delta(L) = \lceil 3L^2 - 3/2 \rceil$ for all L. ■

Theorem 1 provides the most efficient way to rigidify quad kirigami: placing links according to the MRPs (see *SI Appendix*, section S1 for a flowchart and the algorithmic procedure of the hierarchical construction method). Moreover, for odd L, since every link in an $L \times L$ MRP decreases the DoF of the kirigami system by exactly two, we can obtain a kirigami with $\mathrm{DoF} = 2k + 3$ by removing exactly k links from an MRP. By adding a link which reduces the DoF by one to such a kirigami system, we can obtain a kirigami with $\mathrm{DoF} = 2k + 2$. For even L, all but one links in an $L \times L$ MRP reduce the DoF of the system by two (except one that reduces the DoF by one). By removing k links from an MRP, we can again obtain a kirigami with $\mathrm{DoF} = 2k + 3$ or $2k + 2$. Therefore, any given DoF is achievable.

Minimum Connecting Link Patterns. For the connectivity of kirigami, a similar question arises: What is the minimum number of prescribed links for making an $L \times L$ kirigami connected? Obviously, when one link is added, the NCC decreases by either zero or one. Define $\gamma(L)$ as the minimum number of links required for connecting an $L \times L$ kirigami, and a minimum connecting link pattern (MCP) to be a link pattern with exactly $\gamma(L)$ links which connects the $L \times L$ kirigami. Note that there are L^2 connected components if all of the links are disconnected, and one connected component if all of the links are connected. Following the same argument as the section above, we have $L^2 - \gamma(L) \leq 1$, and thus $\gamma(L) \geq L^2 - 1$. It turns out that, by explicit construction, we are able to show that this lower bound is optimal for all L.

Theorem 2 *For all positive integers* L, $\gamma(L) = L^2 - 1$.

(See *SI Appendix*, section S2 for the detailed proof.) Similar to the construction of MRPs, the construction of MCPs can be done by hierarchical construction. Besides, since every link in an MCP decreases the NCC by exactly one, we can obtain a kirigami with $k + 1$ connected components by removing k links from an MCP. Therefore, *Theorem 2* provides us with an efficient way for constructing a kirigami system with any given NCC.

From *Theorems 1* and *2*, we can easily see that, for $L \geq 2$,

$$\delta(L) = \left\lceil \frac{3L^2 - 3}{2} \right\rceil > L^2 - 1 = \gamma(L). \qquad [6]$$

This implies that there is no MRP which is also an MCP for $L \geq 2$. It also suggests that, in general, rigidifying a kirigami requires more effort (links) compared to connecting the quads in kirigami. We remark that, by using MRPs and MCPs, we can achieve a certain level of simultaneous control of rigidity and connectivity. For instance, we can achieve an $L \times L$ system with $\mathrm{NCC} = d^2$ and $\mathrm{DoF} = 3d^2$ precisely if d is a factor of L (see *SI Appendix*, section S4 for a detailed discussion).

Enumeration of Minimum Link Patterns. It is noteworthy that the constructions of MRPs and MCPs are not necessarily unique. Denote the number of MRPs and MCPs in an $L \times L$ kirigami by $n_r(L)$ and $n_c(L)$, respectively. To obtain $n_r(L)$, note that the total number of links in an $L \times L$ kirigami is $4L(L-1)$, and hence there are $\binom{4L(L-1)}{\lceil 3L^2 - 3/2 \rceil}$ possibilities to examine. As this number grows rapidly with L, obtaining $n_r(L)$ by direct enumeration is nearly impossible. Nevertheless, we can make use of the hierarchical construction to obtain a lower bound of $n_r(L)$ (*SI*

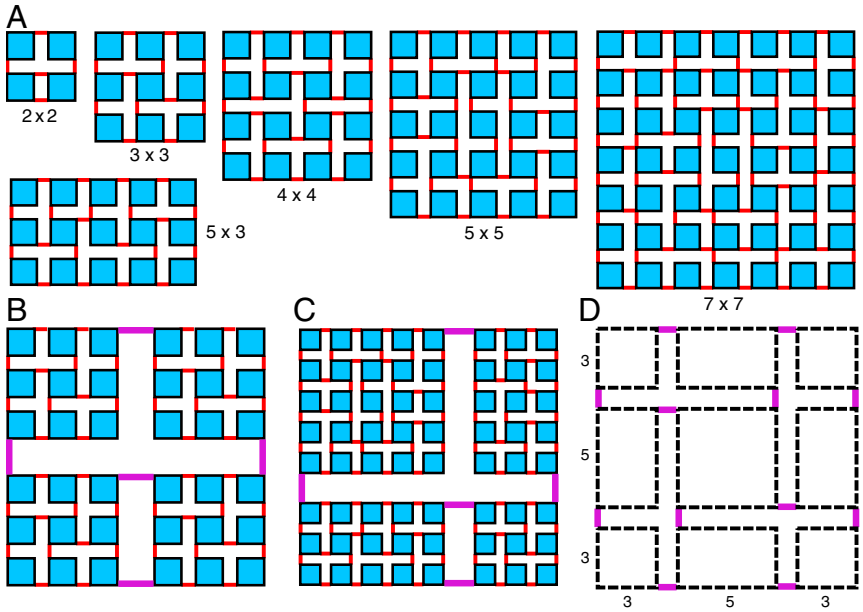

Fig. 2. The construction of MRPs. (*A*) Explicit construction of MRPs for $L = 2, 3, 4, 5, 7$, and for 3×5. (*B*) The construction of an MRP for $L = 6$ using hierarchical construction. The 6×6 kirigami is decomposed into four large blocks of size 3×3. Each large block is rigidified using an MRP for $L = 3$ (red links), and then the four large rigid blocks are linked and rigidified using an MRP for $L = 2$ (purple links). (*C*) The construction of an MRP for $L = 2^k$, $k \geq 3$ using hierarchical construction. A $2^3 \times 2^3$ kirigami is decomposed into large blocks of size 3×3, 5×5, and 3×5. Each large block is rigidified using an MRP (red links), and then the four large rigid blocks are linked and rigidified using an MRP for $L = 2$ (purple links). (*D*) The construction of an MRP for odd primes $p \geq 11$ using hierarchical construction. A 11×11 kirigami is decomposed into large blocks of size 3×3, 5×5, and 3×5. Each large block is rigidified using an MRP, and then the four large rigid blocks are linked and rigidified using an MRP for $L = 3$ (purple links).

Appendix, section S1 and Table S1). Similarly, for $n_c(L)$, there are $\binom{4L(L-1)}{L^2-1}$ possibilities to examine, which becomes impossible for enumeration for large L. This time, we can make use of the Kirchhoff's matrix tree theorem (23) to obtain $n_c(L)$ (*SI Appendix*, section S2 and Table S2). Comparing $n_r(L)$ and $n_c(L)$, we observe that there are many more MCPs than MRPs, suggesting that it is much easier to connect a kirigami than to rigidify a kirigami.

Note that both $n_r(L)/\binom{4L(L-1)}{\lceil 3L^2-3/2\rceil}$ and $n_c(L)/\binom{4L(L-1)}{L^2-1}$ become extremely small as L increases (*SI Appendix*, Tables S1 and S2). This suggests that, for large L, it is almost impossible to obtain an MRP (or MCP) by randomly picking $\lceil 3L^2-3/2\rceil$ (or L^2-1) links. Thus, our hierarchical construction is a powerful tool for rigidifying or connecting a large kirigami, and for further achieving a given DoF or NCC, with the minimum amount of materials (links).

Kirigami with Random Cuts

Controlling the link patterns (locations) according to MRPs and MCPs is a powerful tool to control rigidity and connectivity, but requires exquisite control of every link at the microscopic level, which is difficult to achieve. A natural question that then arises is, what if we cannot control the microscopic details of the link patterns? Could we still achieve connectivity and rigidity control by only tuning the fraction of randomly added links in the linkage graph?

Connectivity Percolation. We start by defining the link density for an $L\times L$ kirigami to be $\rho(L)=c/c_{\max}$, where c is the number of randomly added links and $c_{\max}=4L(L-1)$ is the maximum number of links. Furthermore, we state that two quads are connected as long as one of the links between them is present, and a connected component is defined as a set of quads among which every two of the quads are connected by a series of links. To study the NCC in quad kirigami with c random links (or equivalently, $(c_{\max}-c)$ random cuts), we denote the NCC in the $L\times L$ kirigami by T, noting that, when $c=0$, $T=T_{\max}=L^2$, while, when $c=c_{\max}$, $T=T_{\min}=1$.

To understand what happens at intermediate values of the density, we randomly generate link patterns and calculate $T(\rho)$ (Fig. 3 *A*–*C*). Initially, each of the randomly added links simply connects two quads, so T decreases by one as each link is added, that is, linearly (Fig. 3*D*). Eventually, however, they are more likely to be added within one connected component rather than between two connected components, as there are more possible positions for adding links within each connected component, and, indeed, the decrease of DoF becomes sublinear (Fig. 3*D*). If we rescale T by $T_{\max}$, we see an exponential decay starting at $\rho=0.3$, finally approaching $1/L^2$ (Fig. 3 *D*, *Right Inset*). We also see that the linear–sublinear transition is universal regardless of the system size L (Fig. 3 *D*, *Left Inset*).

Furthermore, we notice that, at the onset of the exponential decay region, the size of the largest connected component (denoted by N) shows percolation behavior. If we rescale N by $N_{\max}=L^2$, we see that N/L^2 switches from zero to one as the largest connected component suddenly becomes dominant (Fig. 3 *A* and *B*, orange quads), and the transition becomes sharper with increasing system size L. Numerically, using the curve for $L=100$, we find that the critical transition point is at $\rho_c^*\approx 0.298$ (Fig. 3*F*).

We can also calculate this transition density ρ_c analytically using the dual lattice method (24). In fact, this ρ_c is the same as the transition density of connectivity percolation of a network, if we consider the kirigami system as a doubly linked network, with quads being nodes and links being edges. Since percolation in a random connecting network is a state where there is a connected path from one side to the other, the probability of percolation is equal to the probability of not having percolation in the dual lattice (*SI Appendix*, section S3). The probability of connecting two quads is $\rho^2+2\rho(1-\rho)$, assuming that each link is equally likely to be connected with probability ρ. The probability of these two quads not being connected is thus $(1-\rho)^2$. Denoting the probability of percolation by $P[x]$ where x is the quad connecting probability, we have $P[\rho^2+2\rho(1-\rho)]=1-P[(1-\rho)^2]$. If we let $\rho^2+2\rho(1-\rho)=(1-\rho)^2$, we obtain $\rho_c=1-\frac{1}{\sqrt{2}}=0.293$. Since the percolation density of having a connected path is the same as when the size of the largest cluster becomes dominant, ρ_c coincides with the percolation threshold of N, which agrees well with our numerical result $\rho_c^*\approx 0.298$.

DoF with Randomly Allocated Links. Moving from the connectivity to the modes of motion (DoF) in the structure, we denote the dependence of DoF on link density by $m(\rho)$. These floppy modes can be further classified into two types: type a, internal modes (Fig. 1 *C* and *D*), the internal rotational modes associated with the movement of some quads with respect to others within one connected component, and type b, rigid-body modes (Fig. 1 *E* and *F*), the two translational motions and one rotational motion of each connected component.

Type a are the floppy modes that correspond to the nontrivial internal modes of rotation which are hard to find and visualize without using the infinitesimal rigidity approach. Since each connected component has three (type b) rigid-body motions (3 DoF), the number of internal DoF is equal to the total DoF minus the NCC multiplied by 3, that is, $m_{\text{int}}=m_{\text{tot}}-3T$.

With varying ρ, the total DoF follows a trend similar to that of the NCC (T). When $\rho=0$, the total DoF is $3L^2$. When a few links are added initially, they are independent constraints, each reducing the DoF by two, and so we see a linear decrease of DoF (Fig. 3*E*). As more links are added, cooperativity between the links sets in and the decrease of DoF becomes sublinear, and shows exponentially decaying behavior similar to that of T: $\log_{10} m\approx -6.0\rho+1.4$ (Fig. 3 *E*, *Right Inset*). Finally, when most links are added, the system becomes rigid, and the DoF approaches three. If we rescale the DoF by the maximum DoF ($m_{\max}=3L^2$) for each L, all of the curves for internal modes collapse (Fig. 3 *E*, *Left Inset*), suggesting that we can control the internal mechanisms in a scale-free manner by simply tuning the link density.

Given the similarity of our system to 2D random networks (16), it is perhaps unsurprising to see this percolation behavior. Indeed, if we plot the second derivative of m as a function of constraint number, we can see that this value has a peak between 0.4 and 0.5. As the system size becomes larger, it converges to $\rho_r=0.429$ (Fig. 3*G*). This behavior qualitatively agrees with the second-order transition in the generic rigidity percolation in two dimensions (16). Quantitatively, an analogy from the MRP/MCP might explain this: Since $\delta(L)/\gamma(L)\approx 3/2$ when L is large, we expect that $\rho_r=3\rho_c/2$ so that $\rho_r=0.439$, which agrees well with our numerical result.

When all of the quads are separated, there are no internal modes, while, when all of the links are connected, the whole system is rigid, and there are no internal modes either. Therefore, the number of internal DoF must be nonmonotonic as links are added, with a local maximum in the number of internal DoF as a function of ρ (see the schematic plot in Fig. 3 *A*–*C*). Indeed, as shown in Fig. 3*E*, the internal DoF first increases as the number of links increases, approaches the number of total DoF, and decreases together with the total DoF as link density further increases. As the density $\rho_i\approx 0.26$, there are maximal number of internal modes, which is different from the density $\rho_c\approx 0.293$, when the whole system first gets almost fully connected. Thus, it is in the neighborhood of $\rho\approx\rho_c$ where we find a range of interesting behaviors as the kirigami structure becomes

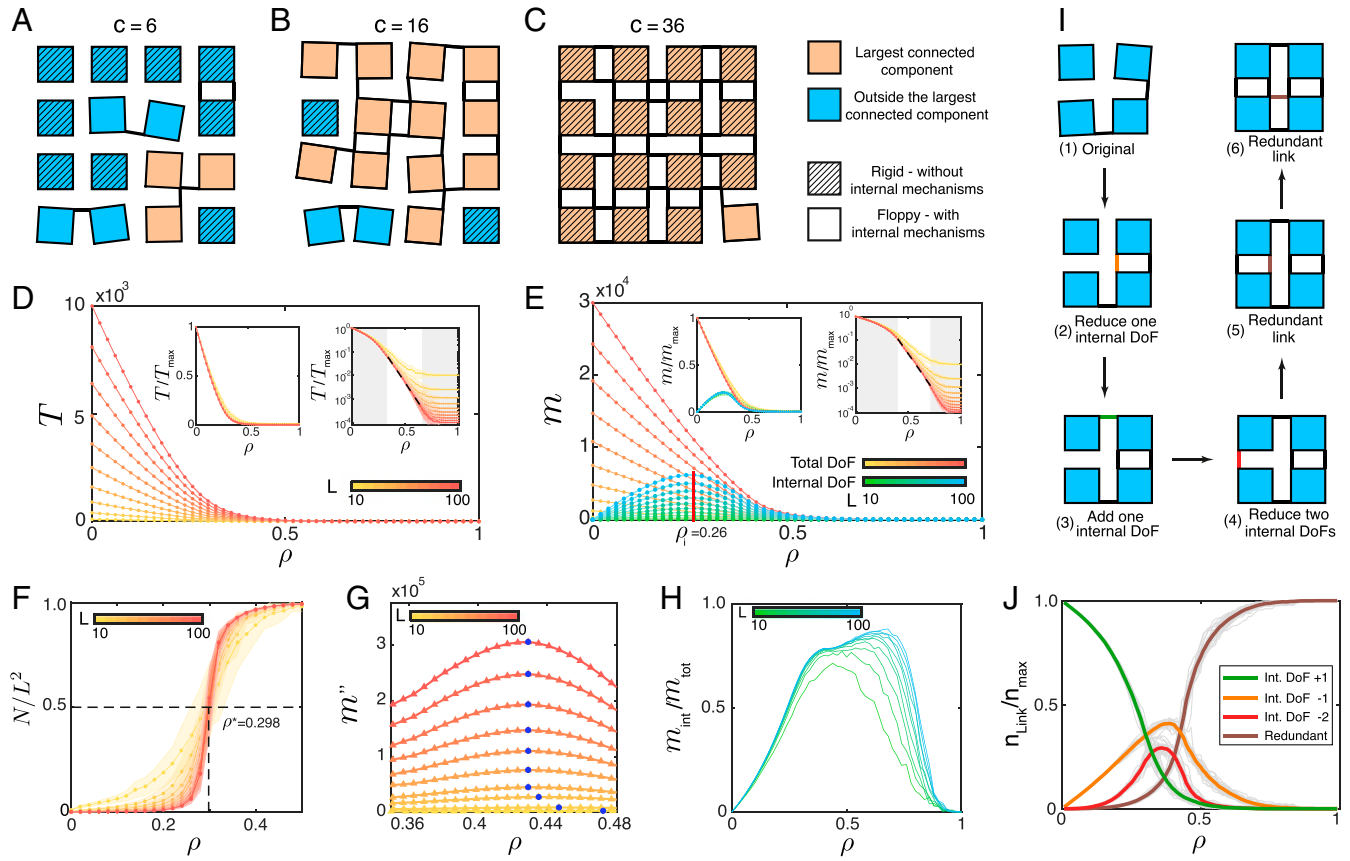

Fig. 3. Connectedness and rigidity of kirigami patterns. (*A*–*C*) For an $L \times L = 4 \times 4$ planar kirigami, links are added randomly. The largest connected component becomes dominant just after a few links are added (orange quads in *B* and *C*). The number of internal modes first increases, then decreases. The number of quads with internal mechanisms (not marked by stripes) first increases before decreasing (*A* to *C*). (*D*) The NCC $T(\rho)$ decreases as link density ρ increases, first linearly, then exponentially at some intermediate ρ (*Right Inset*) before flattening out. This exponential behavior is independent of system size L—if T is scaled by $T_{\max}$ (*Left Inset*). (*E*) The change of DoF ($m(\rho)$) shows a similar linear–sublinear transition, exponential decay (*Right Inset*) and the scale independence (*Left Inset*) as NCC. The number of internal mechanisms increases, reaches a peak at $\rho_i = 0.26$, and approaches the m_{tot} while decreasing. (*F*) The size of the largest cluster (N) has a percolation behavior near $\rho = 0.298$. The transition becomes sharper for larger L. (*G*) The second derivative of total DoF has a peak at the rigidity percolation threshold. The blue dots represent the peak of each curve, the values of which converge to 0.429. (*H*) The ratio of the number of internal mechanisms and the number of total mechanisms as a function of ρ. The internal mechanism dominates from $\rho \in (0.4, 0.8)$. (*I*) An example showing how the links can affect DoF (rigidity) and T (connectivity) in planar kirigami. From the initial state 1, adding the orange link in state 2 reduces one internal DoF ($\Delta_i = -1$, $\Delta_r = 0$). In state 3, the green links reduces the NCC, but there is one more internal mechanism ($\Delta_i = +1$, $\Delta_r = -3$). In state 4, the red link freezes the two internal mechanisms, making the system rigid ($\Delta_i = -2$, $\Delta_r = 0$). Finally, in states 5 and 6, the link added is redundant. Neither type of DoF is changed ($\Delta_i = 0$, $\Delta_r = 0$). (*J*) For a system of size $L = 30$, as links are added randomly, their influence on DoF is shown in terms of the proportion of each type of link in *A* during this process.

almost fully connected, while the number of internal mechanisms remains large (similar to the diluted rotating square system as described in a recent paper (19); see *SI Appendix*, section S3 for more details). Indeed, from the ratio of the internal DoF and the total DoF $m_{\text{int}}/m_{\text{tot}}$ (Fig. 3*H*), we see that the fraction of internal DoF is large for a range of link density, consistent with the intuition that there are more rotational modes within each connected component of kirigami than rigid-body modes of the component.

Constraint Redundancy. We have seen that, when links are added to the system, they do one of three things: change the total DoF, change the internal DoF, or are simply redundant. This notion is generic to a number of different systems made of discrete components with constraints; indeed, recently, we showed that this is also true for origami (20). To address the question here, instead of randomly generating link patterns, we start with no links and add links one by one. At each step, if the DoF of the system does not change after a link is added, we define this link as a redundant link. Otherwise, we define it to be nonredundant. We can further classify these nonredundant links by examining how they change the internal DoF. We denote the change of total DoF as Δ_t, the change of rigid-body DoF (type b) as Δ_r, and the change of internal DoF (type a) as Δ_i. It turns out that the only possible combinations of (Δ_i, Δ_r) are $(-2, 0), (-1, 0), (0, 0), (+1, -3)$, the third of which is defined as redundant (*SI Appendix*, section S3). In Fig. 3*I*, we show a schematic of the four types of links classified above. Starting from the original configuration (step 1), there are two connected components, each with three type b DoF. The larger component also has two internal DoF. The orange link, after being added to the kirigami system, reduces one internal DoF (Fig. 3*I*, step 2). The green link connects the two components afterward, so $\Delta_r = -3$, and $\Delta_i = +1$. There is one more internal mode (Fig. 3*I*, step 3). In step 4, the red link freezes the two rotational modes simultaneously, making the whole system rigid. Finally, in steps 5 and 6, the links added are redundant, as they do not change DoF.

We now apply this link-by-link examination to a larger kirigami system with $L = 30$. We define the redundancy r in the system as the ratio of the number of redundant links over the number

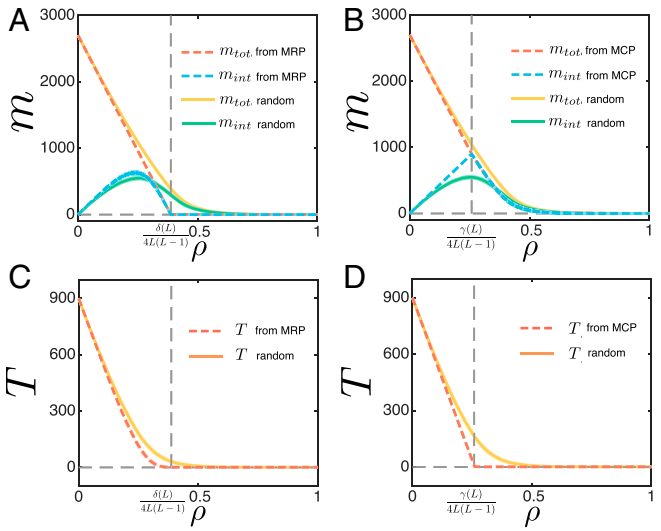

Fig. 4. (*A* and *B*) The change in the total DoF m_{tot} and the internal DoF m_{int} by randomly removing or adding links, starting from (*A*) an MRP or a random link pattern and (*B*) an MCP or a random link pattern. (*C* and *D*) The change in the total NCC T by randomly removing or adding links, starting from (*C*) an MRP or a random link pattern and (*D*) an MCP or a random link pattern.

of all unconnected links. Initially, most of the links are nonredundant, as they are all independent, and each of them adds one internal mode, since they connect two disconnected components (such as Fig. 3*I*, steps 2 and 3). After the connectivity percolation, the links that reduce the internal DoF become dominant, and, eventually, most additional links become redundant. The fraction of redundant links $n_{\text{Link}}/n_{\max}$ has a transition near $\rho = 0.45$ (Fig. 3*J*), consistent with the rigidity percolation threshold ρ_r, suggesting that, after the rigidity percolation, most of the links become redundant. This observation shows how each added link affects the rigidity of kirigami; for example, when $\rho \approx 0.4$, each added link reduces the internal rotational DoF, rather than connecting two connected components, and, when $\rho \approx 0.6$, the system is almost connected and rigid because most new links added will be redundant.

Combining Two Approaches. Deterministic control enables us to achieve certain DoF and NCC precisely based on MRPs and MCPs, while statistical control makes it possible to achieve more combinations of DoF and NCC but only in a random sense. It is natural to ask whether we can combine these two approaches to take advantage of both of them. Given a link density ρ, we start with an MRP (or MCP) and randomly add/remove $4L(L-1)|\rho-\rho_r|$ (or $4L(L-1)|\rho-\rho_c|$) links. The experiment is repeated 100 times, and the average m_{int}, m_{tot}, T, and N for different ρ are recorded.

For DoF, since all links in MRPs are nonredundant, randomly removing links from them results in a linear change of m_{tot} (Fig. 4*A*). More interestingly, starting from an MCP, both adding and removing links randomly result in a decrease of the internal DoF m_{int} (Fig. 4*B*), which can be explained by our construction of MCPs (*SI Appendix*, Fig. S3). In fact, this is the largest internal DoF that can be achieved. For NCC, T increases gradually as links are removed from MRPs (Fig. 4*C*). By contrast, a sharp transition of T can be observed as links are removed from MCPs (Fig. 4*D*). Overall, by combining the deterministic and statistical control, we can achieve a wider range of DoF and NCC, and various behaviors under a perturbation of link density (*SI Appendix*, section S4).

Discussion

Our study of rigidity and connectivity in kirigami was made possible by the realization of a one-to-one mapping between the cutting problem and an equivalent linkage problem. This allowed us to provide a bottom-up hierarchical algorithm to construct MRPs and MCPs, which allow us to rigidify and connect kirigami tessellations optimally. The MRPs and MCPs also provide us with a simple method for obtaining a kirigami system with any given DoF or NCC. Overall, this suggests that we can exquisitely control the rigidity and connectivity of kirigami with the topology of prescribed cuts.

At a more coarse-grained level, we also show how to control connectivity and rigidity by tuning the density of links. We find three critical thresholds: the density for maximum internal DoF (ρ_i), for connectivity percolation (ρ_c), and for rigidity percolation (ρ_r), with $\rho_i < \rho_c < \rho_r$, providing guidance for tuning the link density to achieve different mechanical properties. For example, one can control the ratio of high-frequency and low-frequency modes by choosing the link density above or below the connectivity percolation, since the low-frequency mode sets in when $\rho > \rho_c$, and the remaining high-frequency modes decrease significantly once $\rho > \rho_r$, the rigidity percolation threshold, with relevance for mechanical allostery (25, 26). Alternatively, since more and more links become redundant when $\rho > \rho_i$, it is possible to change the DoF by rearranging the positions of links. For example, according to Fig. 3*J*, if we remove redundant links (brown) and add links that reduce the internal DoF by 1 (red), we reduce the total DoF by 1 while keeping the total number of links the same, thereby changing the DoF information using the same amount of materials; indeed this might allow for click kirigami (i.e., with reversible links) to be a substrate for mechanical information storage, similar to origami (20).

In a broader context, our theoretical study on the rigidity and connectivity in kirigami complements recent developments in the design and fabrication of physical kirigami structures (8, 27–30), by providing guidelines for their control via internal rotational mechanisms, similar to that seen in origami (31). Two natural future paths are to investigate functional devices that might exploit this and to explore the generalization of these arguments to 3D kirigami with polyhedra (32) in the context of architectural and structural design.

Data Availability Statement. Codes related to this paper have been deposited in the GitHub repository (https://github.com/garyptchoi/kirigami-control).

ACKNOWLEDGMENTS. This work was supported, in part, by the Croucher Foundation (to G.P.T.C.) and NSF Grants 14-20570 (to L.M.) and DMREF (Designing Materials to Revolutionize and Engineer our Future) 15-33985 (to L.M.).

1. J. N. Grima, K. E. Evans, Auxetic behavior from rotating squares. *J. Mater. Sci. Lett.* **19**, 1563–1565 (2000).
2. J. N. Grima, A. Alderson, K. E. Evans, Negative Poisson's ratios from rotating rectangles. *Comp. Methods Sci. Technol.* **10**, 137–145 (2004).
3. J. N. Grima, A. Alderson, K. E. Evans, Auxetic behaviour from rotating rigid units. *Phys. Status Solidi B* **242**, 561–575 (2005).
4. S. Shan, S. H. Kang, Z. Zhao, L. Fang, K. Bertoldi, Design of planar isotropic negative Poisson's ratio structures. *Extreme Mech. Lett.* **4**, 96–102 (2015).
5. A. Rafsanjani, D. Pasini, Bistable auxetic mechanical metamaterials inspired by ancient geometric motifs. *Extreme Mech. Lett.* **9**, 291–296 (2016).
6. C. L. Kane, T. C. Lubensky, Topological boundary modes in isostatic lattices. *Nat. Phys.* **10**, 39–45 (2014).
7. K. Sun, A. Souslov, X. Mao, T. C. Lubensky, Surface phonons, elastic response, and conformal invariance in twisted kagome lattices. *Proc. Natl. Acad. Sci. U. S. A.* **109**, 12369–12374 (2012).
8. A. Rafsanjani, K. Bertoldi, Buckling-induced kirigami. *Phys. Rev. Lett.* **118**, 084301 (2017).
9. M. K. Blees *et al.*, Graphene kirigami. *Nature* **524**, 204–207 (2015).
10. M. Isobe, K. Okumura, Initial rigid response and softening transition of highly stretchable kirigami sheet materials. *Sci. Rep.* **6**, 24758 (2016).

11. Y. Tang, J. Yin, Design of cut unit geometry in hierarchical kirigami-based auxetic metamaterials for high stretchability and compressibility. *Extreme Mech. Lett.* **12**, 77–85 (2017).
12. H. Mitschke, V. Robins, K. Mecke, G. E. Schröder-Turk, Finite auxetic deformations of plane tessellations. *Proc. R. Soc. Lond. A* **469**, 20120465 (2013).
13. H. M. Kolken, A. A. Zadpoor, Auxetic mechanical metamaterials. *RSC Adv.* **7**, 5111–5129 (2017).
14. R. Gatt *et al.*, Hierarchical auxetic mechanical metamaterials. *Sci. Rep.* **5**, 8395 (2015).
15. G. P. T. Choi, L. H. Dudte, L. Mahadevan, Programming shape using kirigami tessellations. *Nat. Mater.* **18**, 999–1004 (2019).
16. D. J. Jacobs, M. F. Thorpe, Generic rigidity percolation: The pebble game. *Phys. Rev. Lett.* **75**, 4051–4054 (1995).
17. D. J. Jacobs, B. Hendrickson, An algorithm for two-dimensional rigidity percolation: The pebble game. *J. Comput. Phys.* **137**, 346–365 (1997).
18. W. G. Ellenbroek, X. Mao, Rigidity percolation on the square lattice. *Europhys. Lett.* **96**, 54002 (2011).
19. L. A. Lubbers, M. van Hecke, Excess floppy modes and multibranched mechanisms in metamaterials with symmetries. *Phys. Rev. E* **100**, 021001 (2019).
20. S. Chen, L. Mahadevan, Rigidity percolation and geometric information in floppy origami. *Proc. Natl. Acad. Sci. U. S. A.* **116**, 8119–8124 (2019).
21. S. Guest, The stiffness of prestressed frameworks: A unifying approach. *Int. J. Solids Struct.* **43**, 842–854 (2006).
22. T. C. Lubensky, C. L. Kane, X. Mao, A. Souslov, K. Sun, Phonons and elasticity in critically coordinated lattices. *Rep. Prog. Phys.* **78**, 073901 (2015).
23. G. Kirchhoff, Über die Auflösung der Gleichungen, auf welche man bei der untersuchung der linearen verteilung galvanischer Ströme geführt wird. *Ann. Phys. Chem.* **72**, 497–508 (1847).
24. D. Stauffer, A. Aharony, *Introduction to Percolation Theory: Revised* (CRC, ed. 2, 1994).
25. L. Yan, R. Ravasio, C. Brito, M. Wyart, Architecture and coevolution of allosteric materials. *Proc. Natl. Acad. Sci. U. S. A.* **114**, 2526–2531 (2017).
26. J. W. Rocks *et al.*, Designing allostery-inspired response in mechanical networks. *Proc. Natl. Acad. Sci. U. S. A.* **114**, 2520–2525 (2017).
27. K. Bertoldi, V. Vitelli, J. Christensen, M. van Hecke, Flexible mechanical metamaterials. *Nat. Rev. Mater.* **2**, 17066 (2017).
28. A. Rafsanjani, Y. Zhang, B. Liu, S. M. Rubinstein, K. Bertoldi, Kirigami skins make a simple soft actuator crawl. *Sci. Rob.* **3**, eaar7555 (2018).
29. D. M. Sussman *et al.*, Algorithmic lattice kirigami: A route to pluripotent materials. *Proc. Natl. Acad. Sci. U. S. A.* **112**, 7449–7453 (2015).
30. Y. Zhang *et al.*, A mechanically driven form of Kirigami as a route to 3D mesostructures in micro/nanomembranes. *Proc. Natl. Acad. Sci. U. S. A.* **112**, 11757–11764 (2015).
31. B. G. G. Chen, C. D. Santangelo, Branches of triangulated origami near the unfolded state. *Phys. Rev. X* **8**, 011034 (2018).
32. M. Kadic, G. W. Milton, M. van Hecke, M. Wegener, 3D metamaterials. *Nat. Rev. Phys.* **1**, 198–210 (2019).

Topological and statistical control of kirigami

Siheng Chen, Gary P. T. Choi, and L. Mahadevan 10.1073/pnas.XXXXXXXXXX

Contents

S1. Rigidity of quad kirigami with prescribed cuts

Determining the DoF of a quad kirigami with a given link pattern.

Edge length constraint For each quad $Q = \{\boldsymbol{x}_1, \boldsymbol{x}_2, \boldsymbol{x}_3, \boldsymbol{x}_4\}$ of an $L \times L$ quad kirigami, there are five constraints concerning length for ensuring the quad is rigid. They consist of four edge constraints and one no-shear constraint:

$$\begin{cases} g_{\text{edge}}(\boldsymbol{x_1}, \boldsymbol{x_2}) = ||\boldsymbol{x}_1 - \boldsymbol{x}_2||^2 - l^2 = 0, \\ g_{\text{edge}}(\boldsymbol{x_2}, \boldsymbol{x_3}) = ||\boldsymbol{x}_2 - \boldsymbol{x}_3||^2 - l^2 = 0, \\ g_{\text{edge}}(\boldsymbol{x_3}, \boldsymbol{x_4}) = ||\boldsymbol{x}_3 - \boldsymbol{x}_4||^2 - l^2 = 0, \\ g_{\text{edge}}(\boldsymbol{x_4}, \boldsymbol{x_1}) = ||\boldsymbol{x}_4 - \boldsymbol{x}_1||^2 - l^2 = 0, \\ g_{\text{edge}}(\boldsymbol{x_1}, \boldsymbol{x_3}) = ||\boldsymbol{x}_1 - \boldsymbol{x}_3||^2 - 2l^2 = 0, \end{cases} \quad [S1]$$

where l is the length of the quad. Therefore, there are in total $5L^2$ length constraints in the $L \times L$ kirigami.

Link constraint For a given link pattern on the $L \times L$ kirigami, each link between two nodes $\boldsymbol{x}_i$ and $\boldsymbol{x}_j$ give one link constraint

$$\boldsymbol{x}_i - \boldsymbol{x}_j = 0, \quad [S2]$$

which can be written as

$$\begin{cases} g_{\text{link}_x}(\boldsymbol{x_i}, \boldsymbol{x_j}) = x_{i_1} - x_{j_1} = 0, \\ g_{\text{link}_y}(\boldsymbol{x_i}, \boldsymbol{x_j}) = x_{i_2} - x_{j_2} = 0, \end{cases} \quad [S3]$$

where $\boldsymbol{x}_i = (x_{i_1}, x_{i_2})$ and $\boldsymbol{x}_j = (x_{j_1}, x_{j_2})$. Therefore, for a link pattern with n links, there are in total $2n$ link constraints.

Calculating DoF We first show that the decrease in total DoF by adding one link is either 0, 1, or 2. Consider a simple example of two separate quads as shown in Fig. S1**a**-**b**. Each quad has 3 DoF (2 translational and 1 rotational). When these two quads are connected by a link (Fig. S1**a**), one of the vertices loses 2 translational DoF and hence the total DoF of them changes from 6 to 4 (change of 2). When the other link is further added between the two quads (Fig. S1**b**), one of the quads loses 1 rotational DoF and hence the total DoF of them changes from 4 to 3 (change of 1). There are also redundant links which do not change the DoF (change of 0) (e.g. ⑤ in Fig. 1B in the main text, assuming all other links are present).

In fact, Fig. S1**a** shows a situation where all of the constraints are independent, and removing any constraint will result in extra DoF(s). Fig. S1**b** shows a situation where the edge length constraint for one of the two edges in between the quads is redundant. This suggests that, in order to calculate the DoF, all the edge length constraints and link constraints should be put together to determine the number of independent constraints.

Therefore, we put all edge length constraints and link constraints in the rigidity matrix $\mathbf{A}$. Each constraint can be written as $g(\boldsymbol{x}) = 0$, where g is a function of the $8L^2$ coordinates of all nodes $\boldsymbol{x}$. Define the rigidity matrix $\mathbf{A}$ to be a $(5L^2 + 2n) \times 8L^2$ matrix where each entry of $\mathbf{A}$ is

$$\mathbf{A}_{ij} = \frac{\partial g_i(\boldsymbol{x})}{\partial x_j}, \tag{S4}$$

and g_i is a length or link constraint ($i \in [1, 5L^2 + 2n]$), and j ranges from 1 to $8L^2$. The matrix is rather sparse, since each link involves at most two nodes (4 coordinates), so there are at most 4 non-zero entries per row in $\mathbf{A}$.

To determine the DoF of the system from the rigidity matrix $\mathbf{A}$, we subtract the number of independent constraints from $8L^2$. In other words, we have

$$\text{DoF} = 8L^2 - \text{rank}(\mathbf{A}). \tag{S5}$$

Detailed proof of Theorem 1. Recall that $\delta(L)$ is defined to be the minimum number of links for rigidifying an $L \times L$ quad kirigami, and a *minimum rigidifying link pattern* (MRP) is defined to be a link pattern with $\delta(L)$ links which rigidifies the $L \times L$ kirigami. Theorem 1 in the main text states that for all positive integer L,

$$\delta(L) = \left\lceil \frac{3L^2 - 3}{2} \right\rceil. \tag{S6}$$

In this section, we give the detailed proof of the above theorem.

For $L = 2, 3, 4, 5, 7$, we have proved the equality by explicitly designing link patterns with $\left\lceil \frac{3L^2-3}{2} \right\rceil$ links (see Fig. 2A in the main text). To verify that they are rigidifying link patterns (i.e. DoF = 3), the rigidity matrix rank computation introduced in the previous subsection is used. The methods for obtaining these patterns are described in Section S6.

For some larger L, we observe that it is possible to construct an MRP by combining the MRPs for smaller L. For example, for $L = 6$, we can treat the 6×6 kirigami as 4 large blocks of 3×3 quads. We take an MRP with 12 links to rigidify every block, and then connect the 4 large blocks by an MRP with 5 links to rigidify the 4 large blocks. This results in a link pattern to rigidify a 6×6 kirigami (see Fig. 2B in the main text), with the total number of links being

$$12 \times 4 + 5 = 53 = \left\lceil \frac{3(6^2) - 3}{2} \right\rceil. \tag{S7}$$

Similarly, for 9×9 we just treat it as 9 large blocks of 3×3 sub-patterns and we can construct a link pattern to rigidify a 9×9 kirigami, with the total number of links being

$$12 \times 9 + 12 = 120 = \left\lceil \frac{3(9^2) - 3}{2} \right\rceil. \tag{S8}$$

The construction of a minimum 12×12, 18×18 and 27×27 kirigami can be done in a similar manner, with the total number of links respectively being

$$12 \times 16 + 23 = 215 = \left\lceil \frac{3(12^2) - 3}{2} \right\rceil. \tag{S9}$$

$$120 \times 4 + 5 = 485 = \left\lceil \frac{3(18^2) - 3}{2} \right\rceil. \tag{S10}$$

$$120 \times 9 + 12 = 1092 = \left\lceil \frac{3(27^2) - 3}{2} \right\rceil. \tag{S11}$$

We call this method of constructing MRPs using the patterns with small size the *hierarchical construction*. More rigorously, the hierarchical construction method suggests the following theorem:

Theorem S1 *For $L = 2^k \prod p_i^{n_i}$ where $k = 0, 1, 2$, p_i are odd primes that satisfy $\delta(p_i) = \left\lceil \frac{3p_i^2-3}{2} \right\rceil$, and n_i are nonnegative integers, we have $\delta(L) = \left\lceil \frac{3L^2-3}{2} \right\rceil$.*

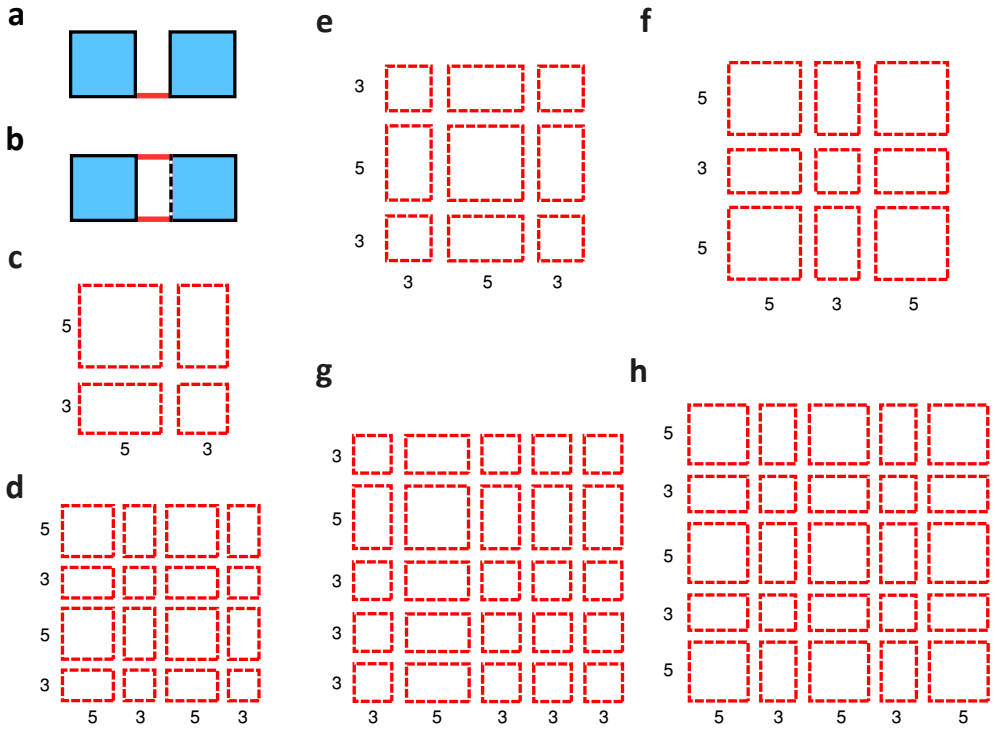

Fig. S1. Constructing minimum rigidifying pattern in quad kirigami. **a**-**b** An example showing that the length constraints might not be independent of the link constraints. **a** When there is only one link between two quads, all of these constraints are independent. **b** When the other link is added, one of the edge length constraint becomes redundant (shown in dashed line). Removing that constraint does not change the DoF. **c** An illustration of the $2^{3-2} \times 2^{3-2} = 4$ large blocks for a $2^3 \times 2^3$ quad kirigami. **d** An illustration of the $2^{4-2} \times 2^{4-2} = 16$ large blocks for a $2^4 \times 2^4$ quad kirigami. The blocks are all with size 5×5, 5×3, 3×5, 3×3. **e**-**h** Possible ways to partition of the 11×11, 13×13, 17×17 and 19×19 quad kirigami patterns into large blocks with size 5×5, 5×3, 3×5, 3×3.

Proof. For $k = 0$, we construct an MRP hierarchically as described below. Suppose L_1, L_2 are two odd numbers satisfying $\delta(L_1) = \left\lceil \frac{3L_1^2-3}{2} \right\rceil$ and $\delta(L_2) = \left\lceil \frac{3L_2^2-3}{2} \right\rceil$. We construct a link pattern for L_1L_2 by treating the $L_1L_2 \times L_1L_2$ quads as $L_2 \times L_2$ large blocks of $L_1 \times L_1$ quads. For every block of $L_1 \times L_1$ quads we use an MRP for L_1 to rigidify the block. Then, for the $L_2 \times L_2$ large, rigidified blocks, we can just consider them altogether as an $L_2 \times L_2$ pattern and use an MRP for L_2 to rigidify them. This hierarchical construction results in a link pattern that rigidifies an $L_1L_2 \times L_1L_2$ kirigami. Note that the total number of links is

$$L_2^2\delta(L_1) + \delta(L_2) = L_2^2 \left\lceil \frac{3L_1^2-3}{2} \right\rceil + \left\lceil \frac{3L_2^2-3}{2} \right\rceil = L_2^2 \frac{3L_1^2-3}{2} + \frac{3L_2^2-3}{2} = \frac{3L_1^2L_2^2-3}{2} = \left\lceil \frac{3L_1^2L_2^2-3}{2} \right\rceil. \quad [S12]$$

This implies that $\delta(L_1L_2) = \left\lceil \frac{3L_1^2L_2^2-3}{2} \right\rceil$. By induction, we can construct an MRP for any $L = \prod p_i^{n_i}$.

For $k = 1$, we first use the above argument to construct an MRP for $\tilde{L} = \prod p_i^{n_i}$. Then, we treat the $2\tilde{L} \times 2\tilde{L}$ quads as 4 large blocks of $\tilde{L} \times \tilde{L}$ quads and rigidify the 4 blocks using an MRP for a 2×2 kirigami. The total number of links in the entire link pattern is

$$2^2\delta(\tilde{L}) + \delta(2) = 4 \left\lceil \frac{3\tilde{L}^2-3}{2} \right\rceil + 5 = 4\frac{3\tilde{L}^2-3}{2} + 5 = \frac{3(2\tilde{L})^2-12+10}{2} = \frac{3(2\tilde{L})^2-2}{2} = \left\lceil \frac{3(2\tilde{L})^2-3}{2} \right\rceil. \quad [S13]$$

For $k = 2$, we first use the above argument to construct an MRP for $\tilde{L} = \prod p_i^{n_i}$. Then, we treat the $4\tilde{L} \times 4\tilde{L}$ quads as 16 large blocks of $\tilde{L} \times \tilde{L}$ quads and rigidify the 16 blocks using an MRP for a 4×4 kirigami. The total number of links in the entire link pattern is

$$4^2\delta(\tilde{L}) + \delta(4) = 16 \left\lceil \frac{3\tilde{L}^2-3}{2} \right\rceil + 23 = 16\frac{3\tilde{L}^2-3}{2} + 23 = \frac{3(4\tilde{L})^2-48+46}{2} = \frac{3(4\tilde{L})^2-2}{2} = \left\lceil \frac{3(4\tilde{L})^2-3}{2} \right\rceil. \quad [S14]$$

■

Corollary 1 *There exists infinitely many L such that $\delta(L) = \left\lceil \frac{3L^2-3}{2} \right\rceil$.*

Proof. By explicit construction of link patterns, we have shown that $\delta(L) = \left\lceil \frac{3L^2-3}{2} \right\rceil$ for $L = 3, 5, 7$. Therefore, the set $\left\{ p_i : p_i \text{ is an odd prime s.t. } \delta(p_i) = \left\lceil \frac{3p_i^2-3}{2} \right\rceil \right\}$ is non-empty. Then, the result follows immediately from the above theorem. ■

Remark: This hierarchical construction method may not work when the sub-patterns are with certain even size. The reason is that the rounding error in $\left\lceil \frac{3(27^2)-3}{2} \right\rceil$ may accumulate and lead to redundant links. For example, treating a 18×18 kirigami as 9 large blocks of 6×6 quads does not result in the optimal lower bound, since in the $L = 6$ case there is redundancy when we add the 5 links for the 2×2 construction.

It is also noteworthy that the construction of MRPs for larger powers of 2 is particularly difficult, as we cannot apply the above idea of hierarchical construction from smaller powers of 2 due to the accumulated rounding error. To overcome this problem, we consider generalizing the above-mentioned hierarchical construction method for rectangular blocks. We first extend the definition of δ for general rectangular kirigami pattern by defining $\delta(M, N)$ as the minimum number of links required for rigidifying a $M \times N$ kirigami. It is easy to see that the lower bound for $\delta(M, N)$ is

$$\delta(M, N) \geq \left\lceil \frac{3MN - 3}{2} \right\rceil. \tag{S15}$$

By explicit construction, we obtained a rigidifying link pattern for 3×5 quad kirigami with 21 links (see Fig. 2A in the main text) and hence we have $\delta(3, 5) = 21 = \left\lceil \frac{3(3\times5)-3}{2} \right\rceil$. With this result, we are ready to prove the following theorem:

Theorem S2 *For any positive integer n, we have*

$$\delta(2^n) = \left\lceil \frac{3(2^n)^2 - 3}{2} \right\rceil. \tag{S16}$$

Proof. We have already proved the case for $n = 1, 2$ by manual construction. We prove the statement for the remaining n by induction. Suppose the statement is true for $n = k - 2$, i.e.

$$\delta(2^{k-2}) = \left\lceil \frac{3(2^{k-2})^2 - 3}{2} \right\rceil. \tag{S17}$$

For $n = k$, we treat the $2^k \times 2^k$ kirigami as $2^{k-2} \times 2^{k-2}$ large blocks with size 5×5, 5×3, 3×5, 3×3 (see Fig. S1**c-d** for an illustration for $k = 3$ and $k = 4$). By taking an MRP for rigidifying each of the blocks and an MRP for rigidifying the $2^{k-2} \times 2^{k-2}$ large blocks, we obtain a link pattern for rigidifying the $2^k \times 2^k$ kirigami. The total number of links is

$$\begin{aligned}
&\frac{2^{k-2} \times 2^{k-2}}{4} \times (\delta(3) + \delta(5, 3) + \delta(3, 5) + \delta(5)) + \delta(2^{k-2}) \\
&= 2^{2k-6} \times (12 + 21 + 21 + 36) + \left\lceil \frac{3(2^{k-2})^2 - 3}{2} \right\rceil \\
&= 45(2^{2k-5}) + 3(2^{2k-5}) - 1 = 48(2^{2k-5}) - 1 = \frac{3(2^k)^2 - 2}{2} = \left\lceil \frac{3(2^k)^2 - 3}{2} \right\rceil.
\end{aligned} \tag{S18}$$

This implies that $\delta(2^k) = \left\lceil \frac{3(2^k)^2-3}{2} \right\rceil$. By induction, the statement holds for all n. ■

Combining Theorem S1 and Theorem S2, it follows that $\delta(L) = \left\lceil \frac{3L^2-3}{2} \right\rceil$ for $L = \prod p_i^{n_i}$ where $p_i = 2, 3, 5, 7, \ldots$ are primes that satisfy $\delta(p_i) = \left\lceil \frac{3p_i^2-3}{2} \right\rceil$ and n_i are nonnegative integers. Note that here we still need to assume the optimality of δ for a prime p_i so as to construct the MRPs for its multiple. To further relax this assumption, we make use of the following lemma:

Lemma 1 *Any odd number $L \geq 11$ can be written as*

$$L = 3m + 5n \tag{S19}$$

where m and n are nonnegative integers.

Proof. Note that $11 = 3 + 3 + 5$, $13 = 3 + 5 + 5$, $15 = 5 + 5 + 5$ and $17 = 3 + 3 + 3 + 3 + 5$. Also, for odd $L \geq 19$, we can express $L = (L - 8) + 3 + 5$. The result follows easily from induction. ■

We then prove the following theorem:

Theorem S3 *For all primes $p \geq 11$,*

$$\delta(p) = \left\lceil \frac{3p^2 - 3}{2} \right\rceil. \tag{S20}$$

Proof. We prove the theorem by induction. Suppose equality holds for all primes less than p. By Lemma 1, there exists nonnegative integers m, n such that $3m + 5n = p$. Since p is odd, $m + n$ is also odd. Also, since $m + n < 3m + 5n = p$, $m + n$ is either an odd prime or a product of odd primes which are smaller than p. It follows from the induction hypothesis, Theorem S1 and Theorem S2 that

$$\delta(m+n) = \left\lceil \frac{3(m+n)^2 - 3}{2} \right\rceil. \tag{S21}$$

Now, we treat the $p \times p$ kirigami as $(m+n) \times (m+n)$ large blocks with size 5×5, 5×3, 3×5, 3×3 (see Fig. S1**e-h** for examples of constructing kirigami with $L = 11, 13, 17$, and 19). By taking an MRP for rigidifying each of the blocks and an MRP for rigidifying the $(m+n) \times (m+n)$ large blocks, we obtain a link pattern that rigidifies the entire $p \times p$ kirigami. The total number of links is

$$\begin{aligned} &m^2\delta(3) + n^2\delta(5) + mn\delta(5,3) + mn\delta(3,5) + \delta(m+n) \\ =&12m^2 + 36n^2 + 42mn + \left\lceil \frac{3(m+n)^2 - 3}{2} \right\rceil \\ =&12m^2 + 36n^2 + 42mn + \frac{3(m+n)^2 - 3}{2} = \frac{3(9m^2 + 25n^2 + 30mn) - 3}{2} = \frac{3(3m+5n)^2 - 3}{2} = \left\lceil \frac{3p^2 - 3}{2} \right\rceil. \end{aligned} \tag{S22}$$

It implies that $\delta(p) = \left\lceil \frac{3p^2-3}{2} \right\rceil$. By induction, the theorem holds for all primes $p \geq 11$. ∎

Finally, using Theorem S1, Theorem S2, Theorem S3 and by induction, we have proved that $\delta(L) = \left\lceil \frac{3L^2-3}{2} \right\rceil$ for all L: If $L = 2^k \prod p_i^{n_i}$ where $k \leq 2$, by Theorem S1 we are done. If $k \geq 3$, we can construct an MRP for $\prod p_i^{n_i} \times \prod p_i^{n_i}$ and an MRP for $2^k \times 2^k$ using the three theorems above. Then, we treat the $L \times L$ quads as 2^{2k} large blocks of $\prod p_i^{n_i} \times \prod p_i^{n_i}$ rigid kirigami and rigidify the 2^{2k} blocks using an MRP for a $2^k \times 2^k$ kirigami. The total number of links in the entire rigidifying link pattern is

$$\begin{aligned} 2^{2k}\delta\left(\prod p_i^{n_i}\right) + \delta(2^k) &= 2^{2k}\left\lceil \frac{3\left(\prod p_i^{n_i}\right)^2 - 3}{2} \right\rceil + \left\lceil \frac{3(2^k)^2 - 3}{2} \right\rceil \\ &= 2^{2k}\frac{3\left(\prod p_i^{n_i}\right)^2 - 3}{2} + \frac{3(2^k)^2 - 2}{2} \\ &= \frac{3\left(2^k \prod p_i^{n_i}\right)^2 - 3(2^{2k}) + 3(2^k)^2 - 2}{2} \\ &= \frac{3L^2 - 2}{2} = \left\lceil \frac{3L^2 - 3}{2} \right\rceil. \end{aligned} \tag{S23}$$

This completes the proof of Theorem 1 in the main text.

As a remark, by Theorem 1 we have

$$\lim_{L\to\infty} \frac{\delta(L)}{\text{Total number of links in an } L \times L \text{ quad kirigami}} = \lim_{L\to\infty} \frac{\left\lceil \frac{3L^2-3}{2} \right\rceil}{4L(L-1)} = \lim_{L\to\infty} \frac{3L^2/2}{4L^2} = \frac{3}{8}. \tag{S24}$$

This implies that for large L, the MRPs for an $L \times L$ quad kirigami use approximately 3/8 of the total number of links.

Algorithmic procedure of the hierarchical construction. As illustrated by the flowchart in Fig. S2, given an arbitrary positive integer $L \geq 2$, the procedure for constructing an MRP for an $L \times L$ quad kirigami is as follows:

1. (Prime factorization) Compute the prime factorization $L = 2^k \prod_{i=1}^m p_i^{n_i}$ where $p_1, p_2, \ldots, p_m$ are distinct odd primes, $k \geq 0$ and $n_i \geq 1$ for all i (see Fig. S2, top left).

2. (MRPs for odd primes) For $p_i = 3, 5, 7$, take the explicitly constructed MRP for $p_i \times p_i$ given in Fig. 2A in the main text. For each $p_i \geq 11$, use the method in the proof of Theorem S3 to construct an MRP for $p_i \times p_i$ with the aid of blocks with size 5×5, 5×3, 3×5, and 3×3 (see Fig. S2, top right).

3. (MRP for the product of all odd prime powers) Use the method in the proof of Theorem S1 to construct an MRP for $p_i^{n_i} \times p_i^{n_i}$ for each i, and subsequently construct an MRP for $\prod_{i=1}^m p_i^{n_i} \times \prod_{i=1}^m p_i^{n_i}$ using the hierarchical construction (see Fig. S2, bottom right).

4. (MRP for the entire kirigami) If $k = 0$ we are done. If $k = 1, 2$, take the explicitly constructed MRP for $2^k \times 2^k$ given in Fig. 2A in the main text. If $k \geq 3$, use the method in the proof of Theorem S2 to construct an MRP for $2^k \times 2^k$ with the aid of blocks with size 5×5, 5×3, 3×5, and 3×3. Finally, apply the method in the proof of Theorem S1 again to construct an MRP for $L \times L$ by rigidifying the $2^k \times 2^k$ large blocks with size $\prod_{i=1}^m p_i^{n_i} \times \prod_{i=1}^m p_i^{n_i}$ (see Fig. S2, bottom left).

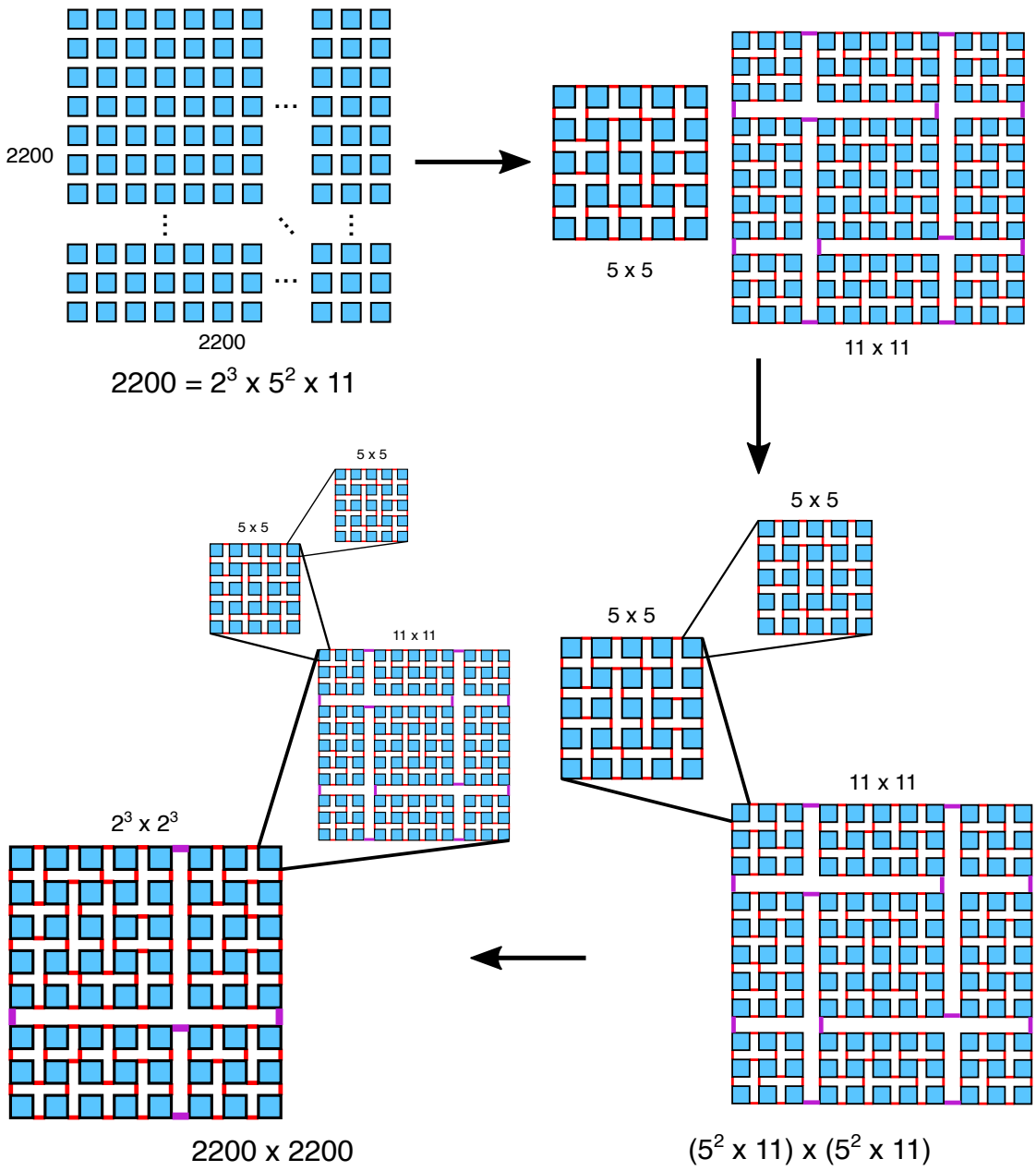

Fig. S2. A flowchart of the hierarchical construction algorithm. To construct an MRP for an $L \times L = 2200 \times 2200$ quad kirigami, we first compute the prime factorization $2200 = 2^3 \times 5^2 \times 11$ (top left). Then, we take the explicitly constructed MRP for 5×5 given in Fig. 2A in the main text, and construct an MRP for 11×11 using the method in the proof of Theorem S3 (top right). After getting MRPs for all prime factors, we construct an MRP for $(5^2 \times 11) \times (5^2 \times 11)$, i.e. the product of all odd prime powers of L, using the method in the proof of Theorem S1 (bottom right). Finally, we use the method in the proof of Theorem S2 to construct an MRP for $2^3 \times 2^3$, i.e. the largest even prime power of L, and subsequently apply the method in the proof of Theorem S1 again to construct an MRP for the entire $L \times L = 2200 \times 2200$ kirigami (bottom left).

We remark that in Step 3 (the construction of MRP for the product of all odd prime powers), the order of the operations is not important: one can either construct an MRP for 11×11 first and then put an MRP for $5^2 \times 5^2$ into each block (as shown in the bottom right of Fig. S2), or construct an MRP for $5^2 \times 5^2$ first and then put an MRP for 11×11 into each block. The order of the operations does not affect the validity of the resulting MRP. However, the operations in Step 4 are not interchangeable: one must use an MRP for the largest power of 2 as the base pattern and put the MRP for the product of all odd prime factors constructed in Step 3 into each block of the base pattern (as shown in the bottom left of Fig. S2). The reason is that changing the order of the operations will violate the derivation for removing the ceiling functions in Eq. (S23), and the resulting number of links will not be $\left\lceil \frac{3L^2-3}{2} \right\rceil$ anymore.

L	$\delta(L)$	Realization	$n_r(L)$	$n_r(L) \Big/ \binom{4L(L-1)}{\lceil (3L^2-3)/2 \rceil} \times 100\%$
2	5	Fig. 2A in the main text	12 (4 if assuming all boundary links)	21.428571%
3	12	Fig. 2A in the main text	140 (10 if assuming all boundary links)	0.005177%
4	23	Fig. 2A in the main text	≥ 182280 (182280 if assuming all boundary links)	$\sim 0.000001\%$
5	36	Fig. 2A in the main text		
6	53	Fig. 2B in the main text	$\geq 140^4 \times 12 \approx 4.6 \times 10^9$	$\ll 0.000001\%$
7	72	Fig. 2A in the main text		
8	95	Fig. 2C in the main text		
9	120	9 blocks with size 3×3	$\geq 140^{10} \approx 2.9 \times 10^{21}$	$\ll 0.000001\%$
10	149	4 blocks with size 5×5		
11	180	Fig. 2D in the main text		
12	215	16 blocks with size 3×3	$\geq 140^{16} \times 182280 \approx 4.0 \times 10^{39}$	$\ll 0.000001\%$
13	252	Fig. S1**f**		
14	293	4 blocks with size 7×7		
15	336	25 blocks with size 3×3 or 9 blocks with size 5×5		
16	383	Fig. S1**d**		
17	432	Fig. S1**g**		
18	485	4 blocks with size 9×9	$\geq (140^{10})^4 \times 12 \approx 8.4 \times 10^{86}$	$\ll 0.000001\%$
19	540	Fig. S1**h**		
20	599	16 blocks with size 5×5		
21	660	49 blocks with size 3×3		
22	725	4 blocks with size 11×11		
23	792	Similar to those in Fig. S1		
24	863	64 blocks with size 3×3		
25	936	5 blocks with size 5×5		
26	1013	4 blocks with size 13×13		
27	1092	9 blocks with size 9×9	$\geq (140^{10})^{10} \approx 4.1 \times 10^{214}$	$\ll 0.000001\%$

Table S1. The optimal lower bound for rigidifying link patterns $\delta(L)$, examples of realization, the number of MRPs $n_r(L)$ and the percentage of MRPs compared to all possible patterns with exactly $\lceil (3L^2-3)/2 \rceil$ links.

Enumeration of minimum rigidifying link patterns (MRPs). Denote the number of MRPs in an $L \times L$ kirigami by $n_r(L)$. Since the total number of links in an $L \times L$ kirigami is $4L(L-1)$ and an MRP must have exactly $\delta(L) = \left\lceil \frac{3L^2-3}{2} \right\rceil$ links, there are in total $\binom{4L(L-1)}{\lceil (3L^2-3)/2 \rceil}$ possible combinations to examine for finding MRPs. For $L = 2$ and 3, by enumeration we can show that there are respectively $n_r(2) = 12$ and $n_r(3) = 140$ MRPs. However, even for just $L = 4$ and 5, there are $\binom{80}{36} \approx 3 \times 10^{13}$ and $\binom{80}{36} \approx 7 \times 10^{22}$ possibilities to examine. This shows that finding the exact number $n_r(L)$ of MRPs is difficult for large L.

One may simplify the computation by assuming that all boundary links are connected. For $L = 2$, with this assumption it is easy to see that there are 4 MRPs. For $L = 3$, we have $\binom{16}{4} = 1820$ combinations, among which we have found 10 MRPs (for simplicity of computation we do not identify patterns with rotational or reflectional symmetry). However, even with this assumption, for $L = 4$ we have $\binom{36}{11} \approx 6 \times 10^8$ combinations to examine, which took us several days to complete the enumeration and obtain 182280 MRPs. For $L = 5$, there are $\binom{64}{20} \approx 2 \times 10^{16}$ combinations, which would require 100 years to finish if each DoF calculation takes 10^{-5} seconds.

Nevertheless, we can make use of our hierarchical construction to obtain a lower bound for the total number of MRPs for some large L. For example, since an MRP for 6×6 can be constructed by treating it as four large blocks of 3×3 quads as shown in Fig. 2B in the main text, there are at least $140^4 \times 12 \approx 4.6 \times 10^9$ MRPs for a 6×6 kirigami. Similarly, we can see that there are at least $140^{10} \approx 2.9 \times 10^{21}$ MRPs for a 9×9 kirigami, $140^{40} \times 12 \approx 8.4 \times 10^{86}$ MRPs for a 18×18 kirigami, and $(140^{10})^{10} \approx 4.1 \times 10^{214}$ MRPs for a 27×27 kirigami.

Table S1 shows a summary of the MRPs for $L = 2, \ldots, 27$. By calculating the percentage of MRPs compared to all the possible patterns with exactly $\lceil (3L^2-3)/2 \rceil$ links, it can be observed that MRPs become more and more rare as L increases. Hence, it is almost impossible to obtain an MRP by trial and error. This shows that the hierarchical construction is important for providing us with explicit examples of MRPs.

S2. Connectivity of quad kirigami with prescribed cuts

After studying the link patterns for rigidifying a kirigami, we proceed to study the link patterns for *connecting* a kirigami, i.e. making it a single connected component.

Detailed proof of Theorem 2. Recall that $\gamma(L)$ is defined to be the minimum number of links for making an $L \times L$ quad kirigami connected, and a *minimum connecting link pattern* (MCP) to be a link pattern with $\gamma(L)$ links which makes the $L \times L$ kirigami connected. Theorem 2 in the main text states that for all positive integer L,

$$\gamma(L) = L^2 - 1. \tag{S25}$$

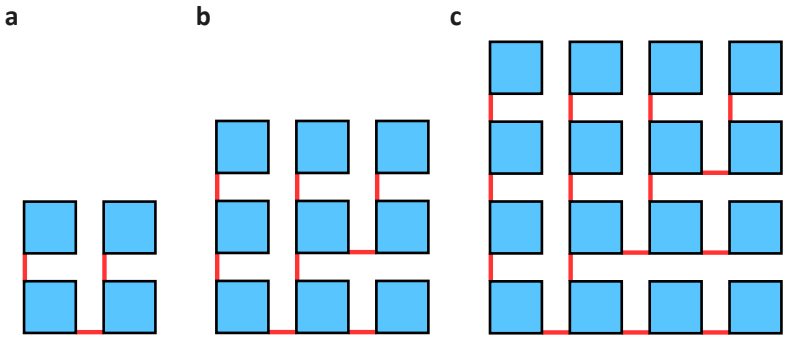

Fig. S3. An illustration of the construction of MCPs for $L \times L$ quad kirigami. Starting from an MCP for $L = 2$ (**a**), we add one link at each edge on the top and the right boundary. This produces an MCP for $L = 3$ (**b**). Repeating the same procedure, we obtain an MCP for $L = 4$ (**c**).

L	$\gamma(L)$	$n_c(L)$	$n_c(L) \Big/ \binom{4L(L-1)}{L^2-1} \times 100\%$
2	3	32	57.142857%
3	8	49152	6.683064%
4	15	3288334336	0.300782%
5	24	9354438770687992	0.005765%
6	35	1.118943×10^{24}	0.000049%
7	48	5.593575×10^{33}	$< 0.000001\%$
8	63	1.164278×10^{45}	$< 0.000001\%$
9	80	1.006628×10^{58}	$< 0.000001\%$
10	99	3.609203×10^{72}	$< 0.000001\%$

Table S2. The optimal lower bound for connecting link patterns $\gamma(L)$, and the number of MCPs $n_c(L)$, and the percentage of MCPs compared to all possible patterns with exactly $L^2 - 1$ links.

We prove the theorem by a constructive proof with induction. Clearly the statement is true for $L = 1$. Suppose it is true for $L = n$. For $L = n + 1$, we first connect the bottom left $n \times n$ quads using the link pattern given by the induction hypothesis. For the remaining $(n + 1)^2 - n^2 = 2n + 1$ quads on the top row and the right column, we add one link at each edge on the top and the right boundary of the $n \times n$ connected kirigami. This adds the remaining n quads on the top and the remaining n quads on the right to the connected component. Finally, we add one more link to connect the top right quad to this component, forming one single connected component of $(n + 1) \times (n + 1)$ quads (see Fig. S3 for an example to construct an MCP for $L = 4$ from an MCP for $L = 2$). The total number of links is

$$n^2 - 1 + n + n + 1 = n^2 - 1 + 2n + 1 = (n + 1)^2 - 1, \tag{S26}$$

and by induction the result follows. ■

It is noteworthy that the hierarchical construction we introduced for obtaining MRPs is also applicable for MCPs. Let m, n be two positive integers. Suppose we have an MCP for $m \times m$ and $n \times n$. If we consider a $mn \times mn$ kirigami as $m \times m$ large blocks of $n \times n$ quads, we can use the hierarchical construction method to obtain a connecting link pattern for the $mn \times mn$ kirigami, with the total number of links being

$$m^2\gamma(n) + \gamma(m) = m^2(n^2 - 1) + (m^2 - 1) = (mn)^2 - 1. \tag{S27}$$

This shows that the constructed link pattern is an MCP for $mn \times mn$.

As a remark, by Theorem 2 we have

$$\lim_{L\to\infty} \frac{\gamma(L)}{\text{Total number of links in an } L \times L \text{ quad kirigami}} = \lim_{L\to\infty} \frac{L^2 - 1}{4L(L - 1)} = \lim_{L\to\infty} \frac{L^2}{4L^2} = \frac{1}{4}. \tag{S28}$$

This implies that for large L, the MCPs for an $L \times L$ quad kirigami use approximately $1/4$ of the total number of links.

Enumeration of minimum connecting link patterns (MCPs). Denote the number of MCPs in an $L \times L$ kirigami by $n_c(L)$. It is possible for us to obtain the exact number $n_c(L)$ of MCPs for an $L \times L$ kirigami using the Kirchhoff's matrix tree theorem. Suppose we construct the Laplacian matrix of the $L \times L$ kirigami by treating the L^2 quads as vertices and the $4L(L - 1)$ possible links as edges. Then, from the Kirchhoff's theorem, the number of MCPs is

$$n_c(L) = \frac{1}{L^2} \prod \lambda_i, \tag{S29}$$

where λ_i are the non-zero eigenvalues of the Laplacian matrix. Table S2 lists the results for $L = 2, \ldots, 10$. Analogous to MRPs, by calculating the percentage of MCPs compared to the all possible patterns with exactly $L^2 - 1$ links, it can be observed

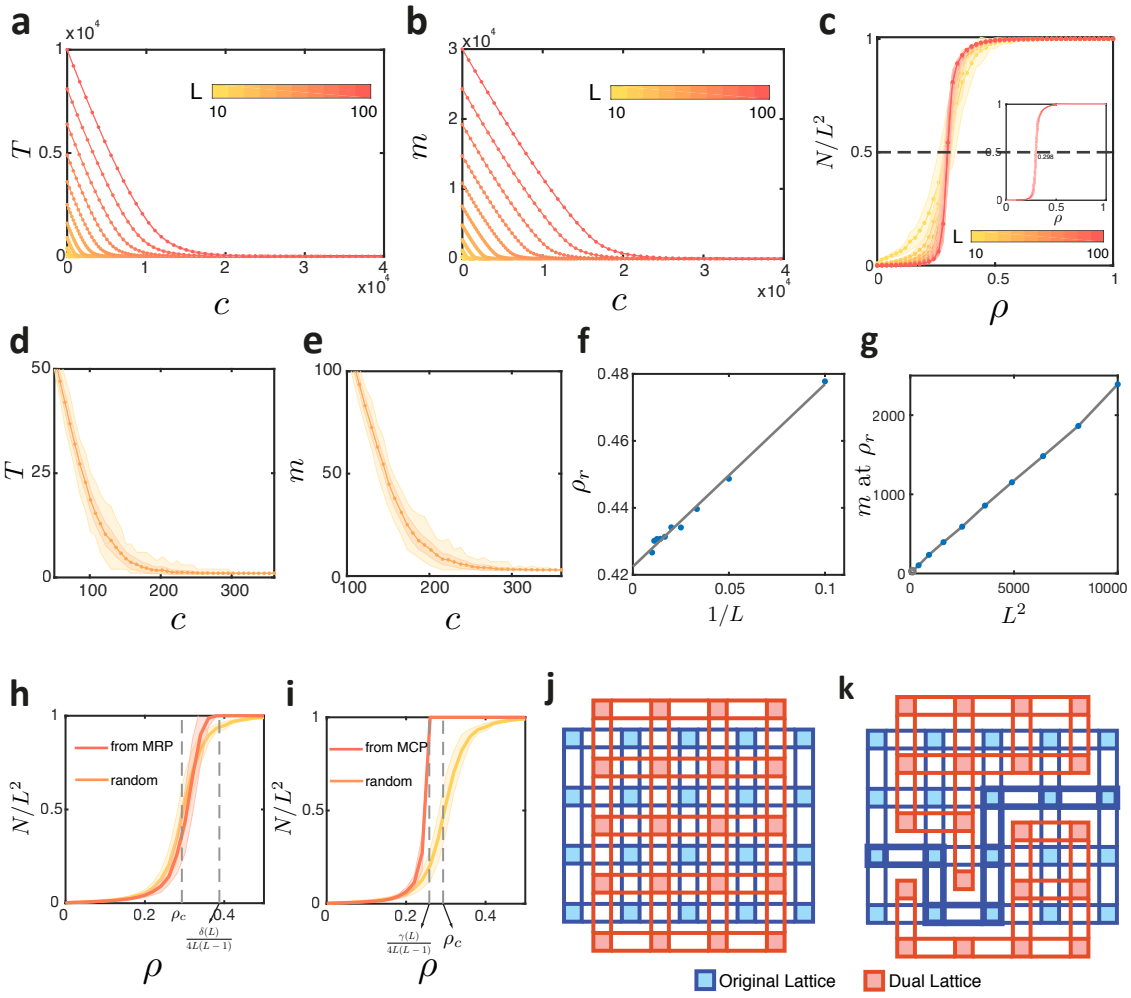

Fig. S4. Connectivity and rigidity of kirigami with random link patterns. **a** For different kirigami with $L = 10, 20, \ldots, 100$, number of connected components decreases first linearly then sub-linearly with the number of links added. The slope in the linear regime is -1. **b** DoF decreases first linearly then sub-linearly with the number of links added. The slope in the linear regime is -2. **g** The portion of the largest connected components in the system with the varying density of links. There is a percolation around 0.3. If we sample densely from 0.1 to 0.5, we can pin down the percolation threshold is $\rho^* = 0.298$ (inset). **d-e** NCC and DoF can vary widely in the sub-linear regime. The lighter shade shows the minimum to maximum, while the darker shade shows the standard deviation. **f-g** The finite size scaling analysis for the rigidity percolation. The peak of the second derivative of m is linear in $1/L$ (**f**), while the peak DoF scales as L^2 (**g**). **h** Starting from MRP (similar to Fig. 4 in main text), the size of the largest connected component is larger than the random case. **i** Starting from MCP, the size of the largest connected component even larger. **j** The dual lattice for calculating the percolation threshold. For the two links connecting two neighboring quads in the original lattice (blue), there are two links in the dual lattice (red) connecting another pair of neighboring quads. **k** When there is percolation in the original lattice from left to right, there is no percolation in the dual lattice from top to bottom.

that MCPs become more and more rare as L increases. Hence, it is almost impossible to obtain an MCP by trial and error. Nevertheless, the hierarchical construction again provides us with a method for explicitly constructing MCPs for large L.

For example, we can treat a 4×4 kirigami as four large blocks of 2×2 quads and perform the hierarchical construction using all possible combinations of MCPs for $L = 2$. This gives $32^4 \times 32 \approx 3.4 \times 10^7$ MCPs, which indicates that there are at least 3.4×10^7 MCPs for $L = 4$. Comparing this result with the exact number $n_c(4) = 3288334336$ given by the Kirchhoff's theorem, we observe that the hierarchical construction is only able to cover around 1% of all MCPs for 4×4. Similarly, for $L = 6$, by hierarchical construction we are able to obtain $49152^4 \times 32 \approx 1.9 \times 10^{20}$ MCPs, which is around 0.02% of the exact number $n_c(6) = 1.118943 \times 10^{24}$ given by the Kirchhoff's theorem. This shows that while the hierarchical construction provides an effective way to construct MCPs, there are still a large number of MCPs which are not covered by this method.

S3. Connectivity and rigidity of quad kirigami with random cuts

Numerical simulations.

Random pattern Recall that the link density of a link pattern for an $L \times L$ kirigami is $\rho = \frac{c}{4L(L-1)}$, where c is the number of links. We vary the link density ρ from 0 to 1. At each given ρ, we randomly generate 200 patterns and calculate the number of connected components, size of the largest connected component, and the DoF using the rigidity matrix calculation described in Section S1.

Calculating number of connected components To calculate the number of connected components (T), we treat the quads as nodes and links as edges, and use the depth-first search algorithm in the resulting network. The size of the largest cluster (N) is the number of quads in the largest cluster. The number of internal DoFs is

$$m_{\text{int}} = m_{\text{tot}} - 3T, \tag{S30}$$

where the factor 3 comes from two rotational DoFs and one translational DoF from each connected component.

Change of connectivity and rigidity.

Linear regime In the main text, we show the change of number of connected components (T) and DoF (m) with the link density. These two quantities first decrease linearly and then sub-linearly. Initially, when ρ is small, most of the quads are disconnected. Adding a link will reduce 1 connected components and 2 DoFs (reducing 3 rigid body DoFs from one connected component, but adding one rotational DoF ($\Delta_i = +1, \Delta_r = -3$). Therefore, if we use the number of links rather than the density as x-axis, the slope of T vs c is -1 (Fig. S4**a**) while the slope of m vs c is -2 (Fig. S4**b**).

Sub-linear regime In the sub-linear region, the average DoF and number of connected components decrease sub-linearly. At each given density, however, the possible values vary in a wide range. In Fig. S4**d-e**, we show the standard deviation, maximum, and the minimum of T and m. The brighter shade shows the range (minimum to maximum), while the darker shade shows the standard deviation. The wide shades suggest that different link patterns with the same number of links can have significantly different DoFs and number of connected components.

Connectivity percolation In a random network where each bond is present with probability p, bond percolation is a state where there is a connected path from one side to the other. It is also the state where the size of the largest connected component becomes dominant in the system. In order to calculate the analytical ρ_c, we transform the N/L^2 percolation into the connecting path percolation problem. To illustrate the process, imagine the quads are shrunk and links are elongated in a kirigami with size $L \times (L+1)$ (Fig. S4**g** blue lattice). Now consider a dual lattice (red) which is the same as the original one, but rotated 90 degrees (or with size $(L+1) \times L$, and aligned properly so that each pair of links in dual lattice is on top of a pair of links in the original lattice except at the boundary. We define the rule of percolation in blue lattice as there is at least one connected path from left to right, and the percolation in the red lattice as having one path from top to bottom. Furthermore, the rule for linking the two neighboring sites in the dual lattice: the two red links between neighbor sites in dual lattice are considered connected when and only when neither of the corresponding blue links are connected in the original lattice.

Therefore, the probability of having percolation in the blue lattice, is equal to the probability of not having percolation in the red lattice, since any horizontal connected path in the blue lattice will block any vertical connected path in the red lattice. For example, Fig. S4**h**) shows a connected path (marked as darker blue) from left to right, which separates the red dual lattice into two parts. Thus, there is no connected path from top to bottom.

Therefore, denote P as the probability of percolation, as a function of the probability of neighbor site connection. Assume that each link is present with probability ρ in the blue lattice, the probability of connecting two neighbors is $\rho^2 + 2\rho(1-\rho)$. (Note that ρ is the link density, and it can be interpreted as the probability that one link is connected.) The probability of having percolation in the blue lattice is thus $P[\rho^2 + 2\rho(1-\rho)]$. On the other hand, in the red lattice, the probability of connecting two neighbors is only when the corresponding two blue sites are not connected: two blue links are not present at the same time with probability $(1-\rho)^2$. Now, based on the definition of the percolation above, we have

$$P[\rho^2 + 2\rho(1-\rho)] = 1 - P[(1-\rho)^2]. \tag{S31}$$

In percolation theory, in the large N limit, the transition is sharp, which suggests that P behaves like a step function near ρ_c. If we let $P[x] = 1/2$, the corresponding x must equal to the critical linking probability.

When $P = 1/2$, we have $P[\rho^2 + 2\rho(1-\rho)] = P[(1-\rho)^2]$, which is equivalent to

$$\rho^2 + 2\rho(1-\rho) = (1-\rho)^2. \tag{S32}$$

Solving this equation yields the critical link density (linking probability)

$$\rho_c = 1 - \frac{1}{\sqrt{2}} = 0.293. \tag{S33}$$

In the main text, we have shown this percolation behavior for different system size L. The percolation happens around 0.3 and the portion of the dominant cluster becomes very close to 1 after 0.5 (Fig. S4**c**). In addition, for $L = 100$, we sample densely from $\rho = 0.1$ to $\rho = 0.5$, and calculate the more accurate numerical ρ_c to be 0.298, which agrees very well with our analytical result (Fig. S4**c** inset).

Rigidity percolation We have shown that the rigidity percolation threshold actually shifts to the left as the system size increases (Fig. 3G in main text). We use a denser sampling to calculate this peak more accurately, and found that the rigidity percolation threshold ρ_r is linear in $1/L$ (Fig. S4**f**). When L is large, it will converge to around 0.422, suggesting that this is a mean-field problem. The DoF at the rigidity percolation threshold scales with L^2 (Fig. S4**g**).

Internal rotational DoF Recently, Lubbers and van Hecke (1) discussed the excess floppy modes in the symmetric geometries compared to the generic case. While our work focuses on other perspectives of rigidity and connectivity and does not consider generic perturbations to the shapes in our system, we find that the excess floppy modes do behave in a similar way as our internal rotational DoF. It might be interesting to start from this "maximally flexible" state, and design multi-branched deformation pathways, similar to that in origami (2, 3).

Redundancy of links and information storage. Each link added to the kirigami may change the DoF and NCC in a different way. As we defined in the main text, Δ_t represents the change of total DoF for a link added, Δ_i shows the change in the internal DoF (type (b)), and Δ_r represents the change in rigid body DoF (type (a)). It follows that $\Delta_t = \Delta_r + \Delta_i$. Since the rigid body DoF is equal to 3 times NCC (T), Δ_r can only have two values $\{0, -3\}$. Δ_t is restricted to $0, -1, -2$, since each link adds at most two independent constraints. In addition, $\Delta_i \leq 1$, since there is at most one additional internal mode added when two clusters connect. Therefore, the only possible combinations of (Δ_i, Δ_r) are $(-2, 0)$, $(-1, 0)$, $(0, 0)$, $(+1, -3)$. When the third case happens, the link is defined as "redundant".

We have shown how the redundancy in the system changes with the link density in the main text. Here we outline the details of this link adding process. Instead of randomly generating link patterns at a given link density, we start from zero link, and add links one by one. At each step, we check whether each of the remaining unconnected links is redundant ($\Delta_t \neq 0$, as defined above). After all of the free links have been checked, we randomly pick one and add the real link. This process is repeated until all the links are added.

In this process, the number of free links n_{free} decreases linearly, and it can be classified into four types $n_{\text{redundant}}$, $n_{\text{int}+1}$, $n_{\text{int}-2}$, $n_{\text{int}+1}$(redundant, reducing internal DoF by 1, reducing internal DoF by 2, increasing internal DoF by 1). As shown in Fig. 4b, the four types of the links have peaks at different link density.

S4. Simultaneous control of rigidity and connectivity

By making use of the MRPs and MCPs constructed using our methods, we can achieve a certain level of control in both rigidity and connectivity by adding links to or removing links from MRPs and MCPs. Below, we describe precisely how NCC and DoF can be controlled simultaneously.

Simultaneous control of NCC and DoF using MRPs. Note that for any $L \times L$ MRP obtained using our hierarchical construction method, adding or removing links that connect the rigid sub-blocks does not change the NCC and DoF within the sub-blocks. Therefore, if d is a factor of L, we can reverse the process of the hierarchical construction and only remove certain "key links" (links that connect the rigid sub-blocks) from the MRP, so that we can control both the NCC and NDoF precisely: It is possible for us to get NCC $= 1, 2, \ldots, d^2$, and at the same time DoF can go from 3 to $3d^2$. During this process, many combinations of NCC and DoF can be achieved.

For instance, consider an MRP of an 18×18 kirigami, which can be constructed by adding $\delta(2) = 5$ key links that connect four sub-blocks of 9×9 MRPs. If we remove one of the five key links connecting the four sub-blocks, the NCC will remain unchanged while the DoF will increase by 1 or 2. By removing two of the five key links, the NCC will remain unchanged or increase by 1, while the DoF will increase by 3 or 4. As the process continues, finally all the five key links are removed and the DoF of each sub-block is 3. Therefore, we achieve a system with NCC $= 4$ and DoF $= 3 \times 2^2 = 12$. To summarize, all possible combinations of NCC and DoF achieved in this process of removing some of the key links from an 18×18 MRP are:

- NCC $= 1$, DoF $= 3$ (original), 4, 5 (removing 1 key link), 6 (removing 2 key links);
- NCC $= 2$, DoF $= 7$ (removing 2 key links), 8 (removing 3 key links);
- NCC $= 3$, DoF $= 9$ (removing 3 key links), 10 (removing 4 key links);
- NCC $= 4$, DoF $= 12$ (removing 5 key links).

In other words, by manipulating only 5 links out of the $\delta(18) = 485$ links in an 18×18 MRP, we can achieve these combinations of NCC and DoF. Furthermore, the above process is also applicable for each of the sub-blocks of 9×9 MRPs. Therefore, our hierarchical construction method for MRPs enables the simultaneous control of NCC and DoF with a large number of combinations.

One may also be interested in changing DoF while keeping NCC as small as possible, which can indeed be achieved by making use of the MRPs obtained using our hierarchical construction method. Recall that in our hierarchical construction method, we always rigidify sub-blocks with odd size, in which each link changes the DoF by exactly 2. Therefore, if we remove a link from any rigid sub-block in an MRP, the DoF will increase by exactly 2 while the NCC will remain unchanged. We can continue this process until the total number of links reaches the connectivity percolation threshold. In other words, NCC $= 1$ and DoF $= 2k + 3$ can be achieved simultaneously by removing k links, where k is small enough such that $\delta(L) - k$ is much higher than the connectivity percolation threshold $(4L(L-1)\rho_c)$ (see the dashed lines in Fig. 4A and 4C in the main text).

Simultaneous control of NCC and DoF using MCPs. As for the MCPs of an $L \times L$ kirigami, we always have NCC $= 1$ and DoF $= 3L^2 - 2(L^2 - 1) = L^2 + 2$ (since each link decreases the DoF by 2, and there are $L^2 - 1$ links in an MCP). By removing each link from an MCP, the NCC increases by 1 and the DoF increases by 2. In other words, we can achieve a system with NCC $= k + 1$ and DoF $= L^2 + 2k + 2$ by removing any k links from an MCP. As for adding a link to an MCP, note that the NCC will not be changed, while the DoF will decrease by 2 until the total number of links reaches the rigidity percolation threshold. Therefore, NCC $= 1$ and DoF $= L^2 - 2k + 2$ can be achieved simultaneously by adding k links to an MCP, where k is small enough such that $\gamma(L) + k$ is much smaller than the rigidity percolation threshold $(4L(L-1)\rho_r)$ (see the dashed lines in Fig. 4B and 4D in the main text).

Simultaneous control using random cuts. The methods above provide a way to precisely control both the DoF and NCC but are limited to certain ranges of link density. When the link density goes beyond those ranges, one can still control the DoF and NCC using Fig. 3D, 3E, and 4 in the main text as a guideline. For example, based on Fig. 3D and 3E in the main text, one can achieve different combinations of DoF and NCC by tuning the link density ρ. In particular, around ρ_i, the internal rotational DoF reaches the maximum. When higher internal rotational DoF is required, or when the condition in the section above $(\gamma(L) + k \ll 4L(L-1)\rho_r)$ does not hold, Fig. 4B still provides the average total DoF and internal DoF in the structure.

In addition, using the same procedure as in Fig. 4 in the main text, we plot the size of the largest connected component as a function of link density (by adding or removing links randomly starting from an MRP or MCP). Since the link density of MCP is smaller than the connectivity percolation threshold (ρ_c), the transition also happens earlier in the MCP case (Fig. S4**i**). Starting from MRP, the connectivity transition is similar to the random case, except that it reaches 1 earlier, as MRP is connected itself.

S5. Extension to kagome kirigami

Our analysis on the rigidity and connectivity of quad kirigami can be extended to kagome kirigami, which consists of triangles instead of quads.

We first study the rigidity and connectivity of the *rectangular kagome kirigami*, in which the number of triangles in each row (and each column) is the same (see Fig. S5**a-e** for examples).

Rigidity of rectangular kagome kirigami with prescribed cuts. Suppose we have an $L \times L$ rectangular kagome kirigami. For the rigidity of rectangular kagome kirigami, we note that there are three edge constraints for each triangle but no no-shear constraint. The construction of the rigidity matrix $\mathbf{A}$ is similar to that with the case of quad kirigami. This time, since there are in total $6L^2$ variables for the coordinates of all nodes, the DoF is given by

$$\text{DoF} = 6L^2 - \text{rank}(\mathbf{A}). \tag{S34}$$

Denote the minimum number of links required for rigidifying an $L \times L$ kagome kirigami by $\delta_\Delta(L)$. Note that the total DoF is clearly $3L^2$, and the introduction of each link can again lead to a change in DoF by $0, 1, 2$. Therefore, we again have the following lower bound for $\delta_\Delta(L)$:

$$\delta_\Delta(L) \geq \left\lceil \frac{3L^2 - 3}{2} \right\rceil. \tag{S35}$$

Analogous to the case of quad kirigami, we can prove that in fact the lower bound is always achievable, i.e.

Theorem S4 *For all positive integer L,*

$$\delta_\Delta(L) = \left\lceil \frac{3L^2 - 3}{2} \right\rceil. \tag{S36}$$

Proof. We use the same approach as in the proof of Theorem 1.

As shown in Fig. S5**a-e**, we first design rigidifying link patterns with exactly $\left\lceil \frac{3L^2-3}{2} \right\rceil$ links for $L = 2, 3, 4, 5, 7$. We have verified these patterns using the rigidity matrix rank computation that the DoF is 3. This shows that $\delta_\Delta(L) = \left\lceil \frac{3L^2-3}{2} \right\rceil$ for $L = 2, 3, 4, 5, 7$. The method for finding these patterns are explained in Section S6.

Then, note that the proof of Theorem S1 is directly applicable in the case of kagome kirigami. Hence, we have established the same result as Theorem S1 for kagome.

Next, we proceed to show that the lower bound can be achieved for $L = 2^n$. Analogous to the proof of Theorem S2, we generalize the definition of δ_Δ for rectangular kagome kirigami with size $M \times N$, and design MRPs for 3×5 and 5×3 kirigami with exactly $\left\lceil \frac{3MN-3}{2} \right\rceil = 21$ links (Fig. S5**f-g**). With these examples, we can decompose a $2^n \times 2^n$ kagome kirigami into blocks of 5×5, 3×3, 5×3 and 3×5 kagome kirigami. Using the MRPs for these sizes and the hierarchical construction, we can prove by induction that the lower bound is achievable for $L = 2^n$ and hence obtain the same result as in Theorem S2.

Finally, we follow the same argument as in the proof of Theorem S3 to prove that the lower bound is achievable for all prime $p \geq 11$. Using all the above results and induction, we have proved that $\delta_\Delta(L) = \left\lceil \frac{3L^2-3}{2} \right\rceil$ for all L. ■

We perform the same procedure as in the previous discussion and consider the enumeration of all MRPs for kagome kirigami. Table S3 summarizes the results. Comparing the number of MRPs for quad and kagome kirigami, one can see that the kagome kirigami possesses less MRPs. This can be explained by the floppiness of the kagome kirigami.

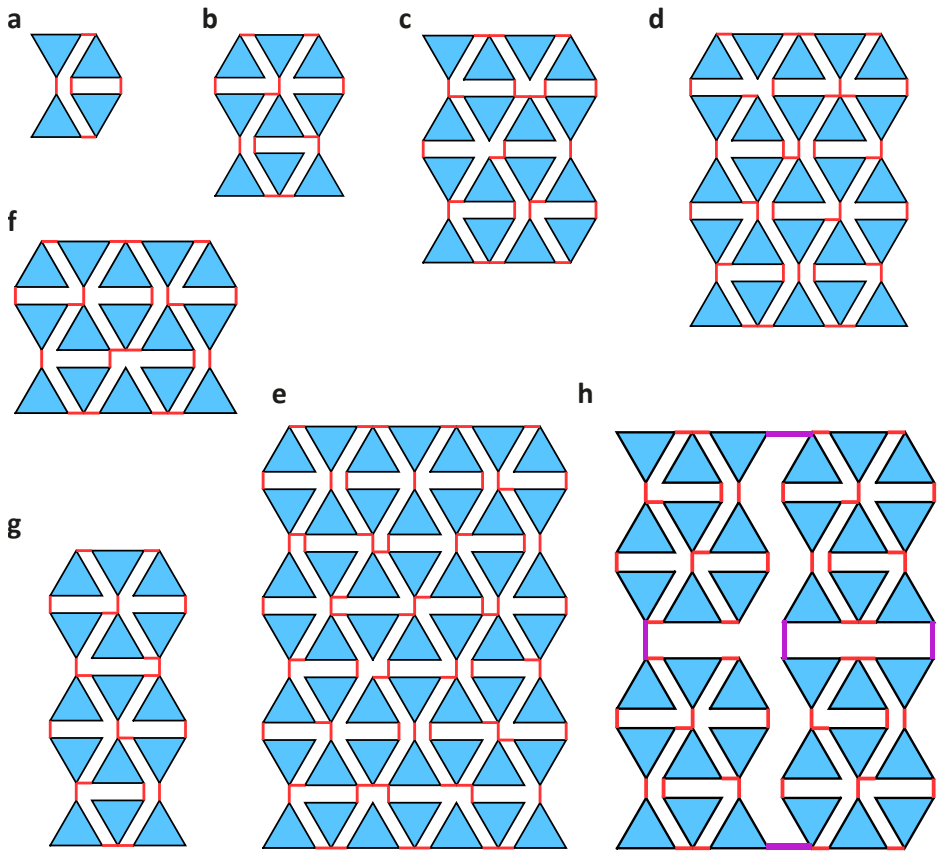

Fig. S5. Explicit construction of MRPs for $L \times L$ rectangular kagome kirigami with $L = 2$ (**a**), $L = 3$ (**b**), $L = 4$ (**c**), $L = 5$ (**d**), $L = 7$ (**e**), and $M \times N$ rectangular kagome kirigami with $(M, N) = (3, 5)$ (**f**), $(M, N) = (5, 3)$ (**g**). **h** An illustration of obtaining MRPs for rectangular kagome kirigami using hierarchical construction. A 6×6 rectangular kagome kirigami can be treated as four large blocks of 3×3 triangles. Each block is rigidified using an MRP for $L = 3$, and then the four large blocks are linked and rigidified using an MRP for $L = 2$. The links altogether form an MRP for $L = 6$.

L	$\delta_\Delta(L)$	Realizations	# MRPs
2	5	Fig. S5**a**	3 (3 if assuming all boundary links)
3	12	Fig. S5**b**	8 (4 if assuming all boundary links)
4	23	Fig. S5**c**	≥ 5324 (5324 if assuming all boundary links)
5	36	Fig. S5**d**	
6	53	Fig. S5**h**	$\geq 8^4 \times 3 = 12288$
7	72	Fig. S5**e**	
9	120	9 blocks with size 3×3	$\geq 8^9 \times 8 \approx 1.1 \times 10^9$
12	215	16 blocks with size 3×3	$\geq 8^{16} \times 5324 \approx 1.5 \times 10^{18}$

Table S3. A table of the optimal lower bound $\delta_\Delta(L)$ for MRPs for rectangular kagome kirigami.

Connectivity of rectangular kagome kirigami with prescribed cuts. Define $\gamma_\Delta(L)$ as the minimum number of links for making an $L \times L$ rectangular kagome kirigami connected, and a *minimum connecting link pattern* (MCP) to be a link pattern with $\gamma_\Delta(L)$ links which makes the $L \times L$ rectangular kagome kirigami connected. As the study of the connectivity for quad kirigami is in fact independent of the geometry of the unit cells, we can repeat the constructive proof of Theorem 2 (see Fig. S6 for an example of construction MCP for $L = 4$ from MCP for $L = 2$) and prove by induction that

Theorem S5 *For all positive integer L,*

$$\gamma_\Delta(L) = L^2 - 1. \qquad [S37]$$

As for the enumeration of all MCPs for rectangular kagome kirigami, the procedure is also analogous to those for quad kirigami. Table S4 summarizes the result.

Rectangular kagome kirigami with random cuts. Similar to the case of quad kirigami, we can study the DoF change with varying link density ρ for rectangular kagome kirigami. Again, the DoF can be classified into two types. From our numerical simulation, we observe a similar behavior as that in quad kirigami: The total DoF decreases first linearly and then sub-linearly

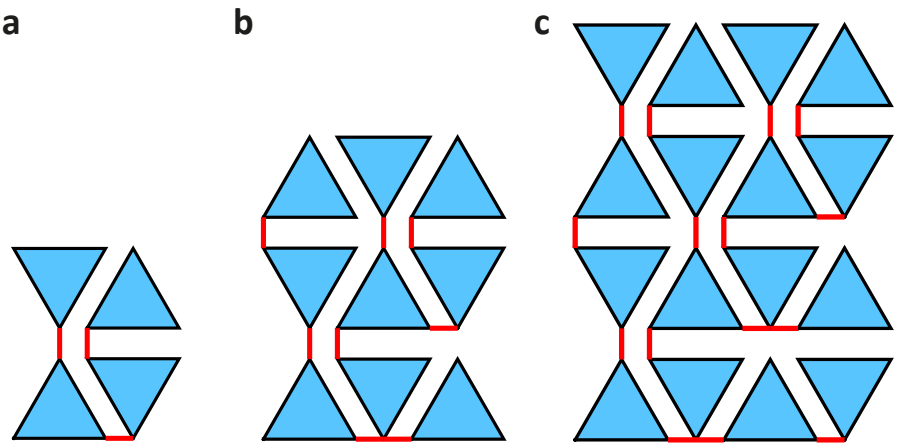

Fig. S6. An illustration of the construction of MCPs for $L \times L$ rectangular kagome kirigami. Starting from an MCP for $L = 2$ (**a**), we add one link at each edge on the top and the right boundary. This produces an MCP for $L = 3$ (**a**). Repeating the same procedure, we obtain an MCP for $L = 4$ (**c**).

L	$\gamma_\Delta(L)$	# MCPs
2	3	20
3	8	14432
4	15	$\geq 20^4 \times 20 = 3200000$
6	35	$\geq 14432^4 \times 20 \approx 8.7 \times 10^{17}$
8	63	$\geq (20^5)^4 \times 20 \approx 2.1 \times 10^{27}$
9	80	$\geq (14432^9) \times 14432 \approx 3.9 \times 10^{41}$
12	143	$\geq (14432^4)^4 \times 20 \approx 7.1 \times 10^{67}$
16	255	$\geq (20^{21})^4 \times 20 \approx 3.9 \times 10^{110}$

Table S4. A table of the optimal lower bound $\gamma_\Delta(L)$ and the number of MCPs for rectangular kagome kirigami.

as the link density increases. The inner rotational DoF first increases, attains the maximum at around $\rho = 0.3$ and then decreases (Fig. S7**a**). The number of connected components (Fig. S7**a**), as well as the proportion of the largest connected components (Fig. S7**b**), have similar behaviors.

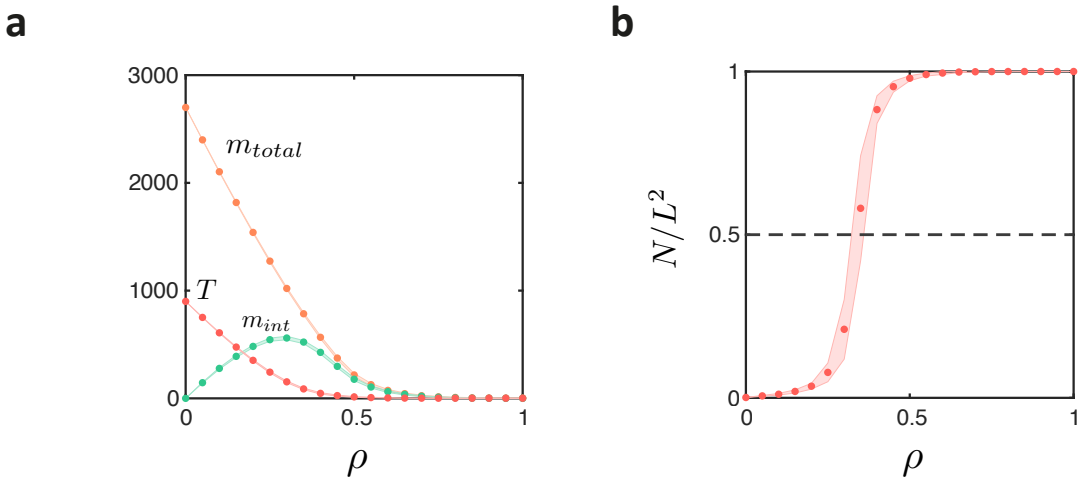

Fig. S7. The connectivity and rigidity of kagome kirigami with random cuts. **a** The change of T, m_{tot}, and m_{rot} with link density, averaged among 200 random link patterns for an $L = 30$ kagome kirigami, follows a similar trend as those is quad kirigami. **b** The proportion of the largest connected components has a similar percolation behavior.

Note that the number of connected components is related to the topology of the kirigami structure. As the topology of the rectangular kagome kirigami and that of the quad kirigami are essentially the same, we omit the study on the number of connected components with varying ρ for the rectangular kagome kirigami here.

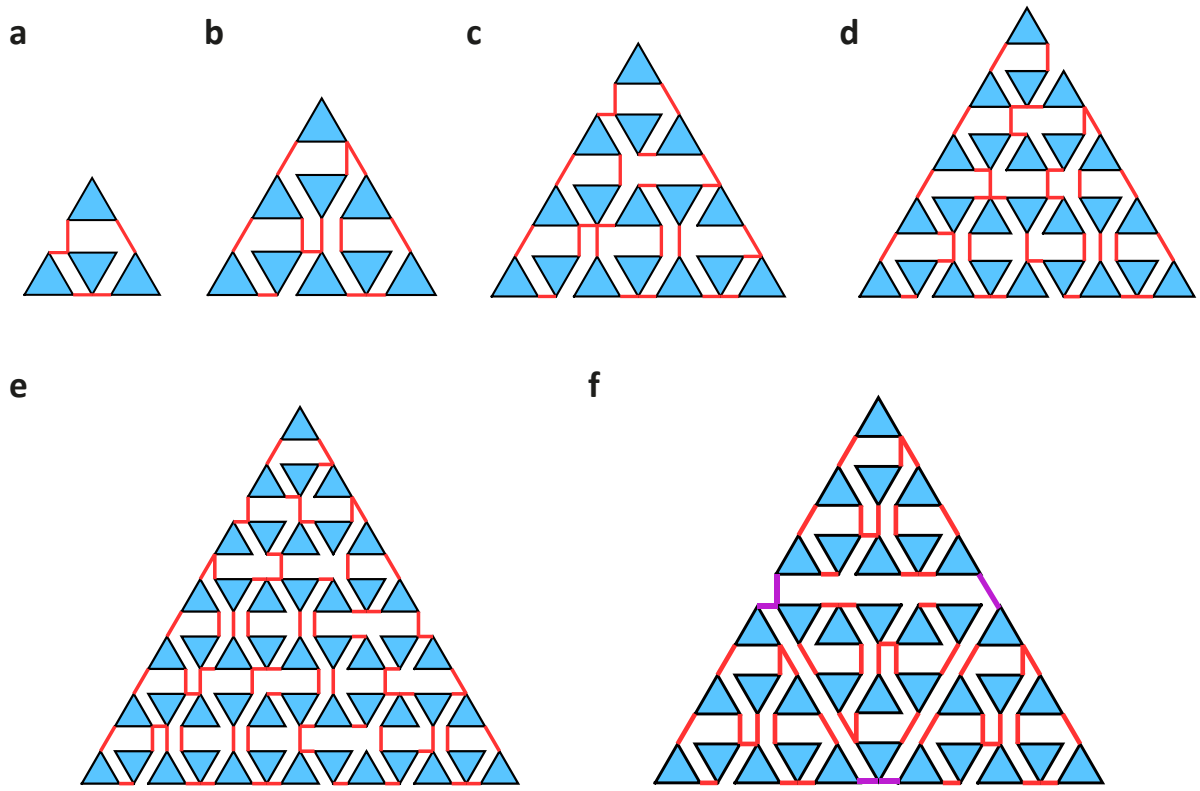

Fig. S8. **a-e** Explicit construction of MRPs for $L \times L$ triangular kagome kirigami with $L = 2, 3, 4, 5, 7$. **f** An illustration of obtaining MRPs for triangular kagome kirigami using hierarchical construction. A 6×6 triangular kagome kirigami can be treated as four large blocks of 3×3 triangles. Each block is rigidified using an MRP for $L = 3$, and then the four large blocks are linked and rigidified using an MRP for $L = 2$. The links altogether form an MRP for $L = 6$.

Triangular kagome kirigami. Besides the rectangular kagome kirigami, we consider another tiling of triangles called the *triangular kagome kirigami*, in which the triangles altogether form a big triangular shape (Fig. S8). For a big triangular shape with side length L, there are in total L^2 triangles. As the theory and construction of MCPs are straightforward, we focus on the construction of MRPs for triangular kagome kirigami for the rest of this section.

Again, we first design rigidifying link patterns with exactly $\left\lceil \frac{3L^2-3}{2} \right\rceil$ links for $L \times L$ triangular kagome kirigami with $L = 2, 3, 4, 5, 7$ (see Fig. S8**a-e**). We have verified these patterns using the rigidity matrix rank computation that the DoF is 3. This shows that $\delta_\Delta(L) = \left\lceil \frac{3L^2-3}{2} \right\rceil$ for $L = 2, 3, 4, 5, 7$. Then, similar to Theorem S1, we can obtain the following result for triangular kagome kirigami:

Theorem S6 *For $L = 2^k \prod p_i^{n_i}$ where $k = 0, 1, 2$, p_i are odd primes that satisfy $\delta_\Delta(p_i) = \left\lceil \frac{3p_i^2-3}{2} \right\rceil$, and n_i are nonnegative integers, then the lower bound for $\delta_\Delta(L)$ for an $L \times L$ triangular kagome kirigami is achievable. In other words,*

$$\delta_\Delta(L) = \left\lceil \frac{3L^2 - 3}{2} \right\rceil. \tag{S38}$$

The proof is the same as the one for Theorem S1. The key idea is to use the hierarchical construction to obtain MRPs from the basic ones. See Fig. S8**f** for an illustration.

However, unlike rectangular kagome kirigami, extending the hierarchical construction method for more general L in the case of triangular kagome kirigami is not straightforward. Recall that the proofs of Theorem S2 and Theorem S3 make use of the decomposition of a kirigami system into large blocks with different sizes (3×3, 5×5, 3×5 and 5×3). Since the topology of rectangular kagome kirigami is essentially the same as that of the quad kirigami, such decomposition can be easily achieved in rectangular kagome kirigami, and the large blocks can be linked and rigidified by an MRP for a smaller L. On the contrary, for triangular kagome kirigami, it is sometimes difficult to define such a decomposition. For example, for $L = 11$, the decomposition used in Theorem S3 involves four 3×3 blocks, one 5×5 block and four 3×5 or 5×3 blocks. We are unable to find any good way to decompose a 11×11 triangular kagome kirigami into such blocks with the hierarchical structure preserved. This suggests that some other approaches may be needed for obtaining the MRPs for those L which are not covered in Theorem S6.

S6. Algorithms for finding MRPs for small L

It is noteworthy that the building blocks of MRPs for both the quad and kagome kirigami are the ones for small $L = 2, 3, 4, 5, 7$, as well as the ones for the rectangular kirigami with $(M, N) = (3, 5), (5, 3)$. The MRPs for these sizes cannot be found by the hierarchical construction. We used two systematic methods for finding MRPs for them.

Method 1: Local Search. We first run a small batch of random trials (say 1000), each with exactly $\delta(L)$ (or $\delta(M, N)$) links chosen, to get an initial link pattern with a relatively low DoF (not necessarily 3). Then, we remove a link from the link pattern to see if the DoF increases by 2. If so, the link is non-redundant with respect to the current link pattern and we add it back to the link pattern. If not, the link is redundant with respect to the current link pattern, and we replace it by another link which further decreases the DoF. The process continues until we get a rigidifying link pattern. As there are multiple possible solutions for MRPs, this local search method turns out to work pretty well in finding an MRP.

Method 2: Pruning. Another possible method is to reject those links that are more likely to be redundant. We start with all the links, and randomly pick one link and put it in a stack. At this stage, since the system is over-constrained, there are 3 DoFs. Assume that those in the stack are the ones rejected (not used in the link pattern).

Each time we calculate the DoF from links outside the stack. If the DoF remains to be 3, we approve this in our stack ("push"), and randomly add a new one (which could be a neighbor or not) in the stack (remove one from the pattern). If the DoF becomes 4 or 5, that means this link is useful (non-redundant), and we remove this in the stack ("pop"). By doing this, we are actually pruning a lot of branches that do not need to be tested. However, sometimes we encounter the situation where all links outside the stack are redundant. That means there should be a link in the stack that might be more useful. When this happens, randomly remove one link from the stack. Finally, when the size of the stack reaches $4L(L-1) - \delta(L)$, algorithm stops and we find the links outside the stack forms an MRP.

All the MRPs of quad kirigami and rectangular kagome kirigami are generated by method 1, and all the MRPs of triangular kagome kirigami are generated by method 2.

1. Lubbers, L. A. & van Hecke, M.. Excess floppy modes and multibranched mechanisms in metamaterials with symmetries. Phys. Rev. E **100**, 021001 (2019).
2. Chen, B. G. G., & Santangelo, C. D.. Branches of triangulated origami near the unfolded state. Phys. Rev. X **8**, 011034 (2018).
3. Pinson, M.B et al. Self-folding origami at any energy scale. Nat. Comm., **8**, p.15477 (2017).